ELSEVIER

Quaternary Science Reviews 26 (2007) 3384–3405

QSR

Quaternary glacial history of the Central Karakoram

Yeong Bae Seong[a], Lewis A. Owen[a,*], Michael P. Bishop[b], Andrew Bush[c], Penny Clendon[d], Luke Copland[e], Robert Finkel[f], Ulrich Kamp[g], John F. Shroder Jr.[b]

[a]*Department of Geology, University of Cincinnati, P.O. Box 0013, Cincinnati, OH 45221-0013, USA*
[b]*Department of Geography and Geology, University of Nebraska—Omaha, 6001 Dodge Street, Omaha, NE 68182-0199, USA*
[c]*Department of Earth and Atmospheric Sciences, University of Alberta, 1-26 Earth Sciences Building, Edmonton, Alberta, Canada T6G 2E3*
[d]*Department of Geography, University of Canterbury, Private Bag 4800, Christchurch, New Zealand*
[e]*Department of Geography, University of Ottawa, 60 University, Ottawa, Ontario, Canada K1N 6N5*
[f]*Center for Accelerator Mass Spectrometry, Lawrence Livermore National Laboratory, Livermore, CA 94550, USA*
[g]*Department of Geography, The University of Montana, SS 204, Missoula, MT 59812-5040, USA*

Received 2 March 2007; received in revised form 18 September 2007; accepted 30 September 2007

Abstract

The Quaternary glacial history of the world's highest mountains, the Central Karakoram, is examined for the first time using geomorphic mapping of landforms and sediments, and ^{10}Be terrestrial cosmogenic nuclide surface exposure dating of boulders on the moraines and glacially eroded surfaces. Four glacial stages are defined: the Bunthang glacial stage (>0.7 Ma); the Skardu glacial stage (marine Oxygen Isotope Stage [MIS] 6 or older); the Mungo glacial stage (MIS 2); and the Askole glacial stage (Holocene). Glaciers advanced several times during each glacial stage. These advances are not well defined for the oldest glacial stages, but during the Mungo and Askole glacial stages glacial advances likely occurred at ~16, ~11–13, ~5 and ~0.8 ka. The extent of glaciation in this region became increasingly more restricted over time. In the Braldu and Shigar valleys, glaciers advanced >150 km during the Bunthang and Skardu glacial stages, while glaciers advanced >80 km beyond their present positions during the Mungo glacial stage. In contrast, glaciers advanced a few kilometers from present ice margins during the Askole glacial stage. Glacier in this region likely respond in a complex fashion to the same forcing that causes changes in Northern Hemisphere oceans and ice sheets, teleconnected via the mid-latitude westerlies, and also to changes in monsoonal intensity.

1. Introduction

The Central Karakoram is an area of significant anomalous topography, which is home to more than sixty peaks that rise above 7000 m above sea level (asl). Four of these peaks exceed 8000 m asl, including K2, the world's second highest mountain at 8611 m asl. The region is also one of the most glaciated tracts outside the polar regions and it contains mountain glaciers that are among the longest ones in the world (e.g., Siachen glacier—70 km long, Biafo glacier—63 km long). The present glaciers occupy deep valleys that descend to <2000 m asl. Thus the area constitutes some of the greatest relative relief on Earth (>5000 m). Impressive successions of moraines and associated landforms are present throughout the valleys of the Central Karakoram. Despite the grandeur of the region no glacial chronologies exist for K2–Baltoro region of the Central Karakoram. The valleys between the town of Skardu in the Indus Valley and K2 were examined in detail to develop a quantitative chronology and to determine the timing and style of glaciation in the Central Karakoram (Fig. 1). Remote sensing techniques, field mapping, sedimentological and geomorphic analysis of landforms, and ^{10}Be terrestrial cosmogenic nuclide (TCN) surface exposure and optically stimulated luminescence (OSL) dating were applied to define the style and nature of glaciation in the region.

2. Physical setting

The Central Karakoram is situated in the Transhimalaya within the Indian–Asian collage collision zone to the north

*Corresponding author. Tel.: +1 513 4102339.
E-mail address: Lewis.Owen@uc.edu (L.A. Owen).

0277-3791/$ - see front matter © 2007 Elsevier Ltd. All rights reserved.
doi:10.1016/j.quascirev.2007.09.015

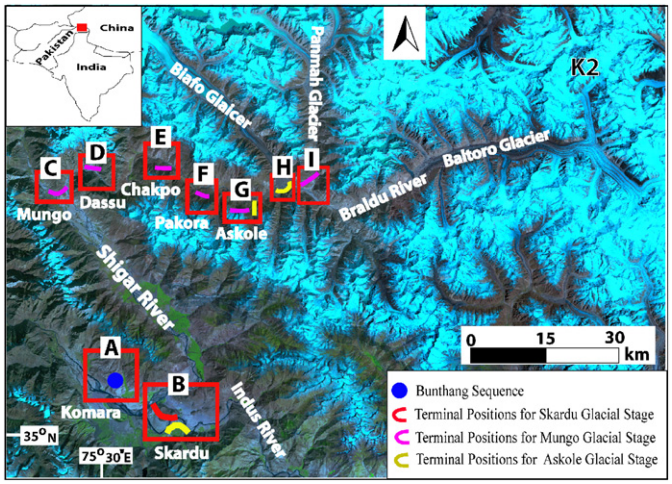

Fig. 1. Mosaicked Landsat ETM+image showing the glaciers in the Skardu–Shigar–Braldu valleys of the Central Karakoram, northern Pakistan. The moraines and terminal positions of the main glacial advances are shown for each glacial stage. The boxes show the locations of the detailed study areas.

of the Nanga Parbat-Haramosh syntaxis and trend northwest along the border of Pakistan and China (Searle, 1991). The main valleys that were examined in this study include part of the Indus, and the Shigar and Braldu valleys. These valleys lead to the Baltoro Glacier, which extends >50 km to K2 and its neighboring peaks, including Broad Peak (8047 m asl), Angel Peak (6858 m asl) and Skil Brum (7360 m asl). The town of Skardu is located in an intermontane basin at the junction of Indus and Shigar valleys and lies at the lowest elevations in the study region at ~2250 m asl (Fig. 1). This basin has thick Quaternary valley fills exceeding several hundreds meters (Owen, 1988; Cronin, 1989; Cronin et al., 1989). The structure and tectonics of the study area are summarized in Searle (1991). Using fission-track dating, Foster et al. (1994) showed that the Central Karakoram, between K2 and the Shigar valley, has experienced an apparent denudation rate of 3–6 mm/a commencing after 5 Ma, with a maximum amount of Pliocene denudation of ⩽7000 m. They estimated that the total amount of denudation at the present mean surface elevation of ~6000 m is ~6000 m.

The hypsometry of the Central Karakoram falls into three distinctive altitudinal zones (Hewitt, 1989). The lower zone below ~3000 m asl is dominated by fluvial processes and comprises gorges and overdeepened valley floors. Most areas are covered by glacial, glaciofluvial, and slope deposits, with thin veneers of aeolian sediment including loess and sporadic dune fields. Paraglacial processes are important in this zone. The middle zone, between 3000 and 6000 m asl, is dominated by glaciated surfaces and mountain ridges. This zone can be further subdivided into active glaciers between 4000 and 6000 m asl and former glacier areas between 3000 and 4000 m asl. The middle zone accounts for most of the surface-area distribution. The upper zone extends above 6000 m asl, comprising the very highest ridges and peaks including K2, Gasherbrum 1 (8068 m), Broad Peak (8047 m), and Gasherbrum II (8035 m). This zone is covered by perennial ice and snow, although numerous bare bedrock slopes are present.

The climate of the region is transitional between central Asian mid-latitude (dominated by the mid-latitude westerlies) and Indian summer monsoon types, and has considerable microclimatic variability influenced by multiscale topographic factors (Owen, 1988; Hewitt, 1989). At Skardu (Fig. 1; 35°18′N, 75°41′E, 2181 m asl), the average annual temperature is 11.5 °C and the mean annual precipitation is 208 mm (averaged for the period 1951–1989 from Meihe et al., 2001). The highest precipitation occurs during spring as the mid-latitude westerlies advance into the region. Two-thirds of snow accumulation on the Central Karakoram occurs in winter and spring, supplied by mid-latitude westerlies, while the other one-third is supplied from the Indian monsoon during summer (Hewitt, 1989). Glaciochemical studies of snow on the Biafo glacier (Fig. 1; 36°40′N, 75°57′E, 4650–5520 m asl; Wake, 1989) show a strong seasonal signal, characterized by relatively higher concentrations of sodium and chlorine in summer snow, indicating that moisture is derived from the Arabian Sea, which is then transported to the mountains by summer monsoonal circulation. In contrast, the winter snow is characterized by overall lower concentrations of sodium and chlorine, reflecting moisture derived from distant marine sources, such as the Mediterranean Sea and/or the Atlantic Ocean. This seasonal contrast of moisture source is also supported by $\delta^{18}O$ values determined for snow from the same glacier (Wake, 1987, 1989). In addition to these two dominating climate systems, continental anticyclones affect the behaviors of the other two systems, which produce strong storms and clear weather conditions (Aizen and Aizen, 1997).

There are more than 30 glaciers over 20 km in length within the Central Karakoram (Fig. 1). The glaciers of the Central Karakoram are characterized by thick debris covers and gradients that vary from very steep (>8°) to gentle (<2°) (Owen and Derbyshire, 1989). Most of the glaciers are of winter accumulation type, whereas in the adjacent Himalayan ranges to the south they are of summer accumulation type, reflecting the difference in the dominant climate system. Excluding the thick debris cover, annual ablation of ice between 3500 and 4500 m asl on the Biafo glacier is of the order of 3000–7000 mm water equivalent (Hewitt, 1989). In particular, snow and ice avalanching are very important in providing mass to their accumulation areas. The intense melting over a period of ~12 weeks during the summer releases most of the annual meltwater, producing proglacial landforms such as outwash terraces, outwash fans and proglacial lakes. There is also a progressive downglacier increase in the amount and thickness of the debris cover in the ablation zones. On some glaciers, such as the Biafo and Baltoro, the lowest stretches are mantled with extremely thick debris, in some places up to 10 m thick. This results in large and cumulative

down-glacier effects on melting, ice-margin conditions and the development of thermokarst forms. Many authors argue that glaciers in this region are probably more responsive to change in precipitation than in temperature and that this characteristic likely extends back into the previous glacial cycles (Derbyshire, 1981; Shi, 2002; Owen et al., 2005).

The altitude effect on precipitation in the Central Karakoram results in an altitudinal zonation of vegetation. Vegetation is scarce along the valley floors and on the lower valley side slopes, which are of desert type, and is replaced with increasing altitudes by temperate coniferous trees and eventually by alpine meadow vegetation. Furthermore, the altitudinal precipitation gradient influences the relative role of Earth-surface processes producing altitudinal variations in the dominant landform patterns and geomorphic processes (Paffen et al., 1956; Hewitt, 1989).

3. Previous glacial geologic studies

Drew (1873) and Dianelli (1922) provided the first descriptions of the glacial geomorphology of the Skardu region. They described Karpochi Rock (sometimes known as the Rock of Skardu) at Skardu and identified tills on its surface. They suggested that a large glacier had extended from the Shigar Valley into Skardu to deposit the tills. Cronin et al. (1989) described a 1.3-km-thick sedimentary succession that is located in the NW corner of Skardu basin, which they named the Bunthang Sequence (Figs. 1A and 2). This sequence comprises a basal diamicton overlain by lacustrine and glaciofluvial sediments. Based on paleomagnetic studies they suggested that the basal till started to accumulate towards the end of the Matuyama chron (ca 0.72 Ma). On the basis of their similar locations, elevations and stratigraphic positions, they correlated it with till exposed on Karpochi Rock (Figs. 1B and 3–5).

Owen (1988) undertook a study of the Quaternary geology of the Skardu basin and provided a reconstruction of the history and extent of glaciation. He recognized four major glacial surfaces throughout the Skardu basin and in the Shigar valley. These were attributed to different glaciations, but they were not named. Owen (1988) suggested that the earliest of these glaciations might predate the Pleistocene. Later, Hewitt (1989, 1999, 2005) highlighted the problems of misidentifying landslide deposits and moraines throughout the Karakoram, and he reinterpreted many of the moraines in the Indus and Shigar valley as catastrophic rock avalanches.

4. Methods

The Skardu basin, the Shigar and Braldu valleys and the Baltoro glaciers were examined and detailed sampling studies were undertaken in nine areas within the region (Fig. 1). This allowed us to examine the glacial and associated landforms and to develop a glacial stratigraphy for the Central Karakoram. Moraines, paraglacial fans, catastrophic flood deposits, and river terraces were mapped in the field aided by remote sensing and correlated morphostratigraphically using the standard techniques of Derbyshire and Owen (1990). The morphostratigraphic relationships between glacial and associated landforms were used to aid in our sampling strategy for dating.

The moraines (m) in each of the study areas (A–I) were assigned a number relative to their age (1 is the oldest). Moraine m_{1A}, for example, is the oldest moraine in study area A and m_{3I} is the youngest moraine in study area I. Using a combination of morphostratigraphy, relative dating and TCN surface exposure dating, broad correlations were made between the valleys studied in the region, and the moraines and the sediments were assigned to one of four glacial stages. Each glacial stage was named after a nearby village (Table 1).

The oldest glacial stage, the Bunthang, comprises highly dissected valley-fill sediments within the Skardu Basin. The next, the Skardu glacial stage, comprises moraines and eroded till on top of mesas within the Skardu Basin and on high ($\gg$1000 m above the valley floor) benches along the lower stretches of the Shigar valley. The next youngest glacial stage, the Mungo, comprises moraines and glacially eroded bedrock surfaces along the Braldu and upper Shigar valley that rise to $>$2000 m above the present valley floors. The youngest glacial stage, the Askole, comprises sharp crested moraines at the heads of tributary valleys along the Braldu valley.

As there is little organic material suitable for ^{14}C dating and if any, most of the deposits are out of range of ^{14}C, we applied ^{10}Be TCN surface-exposure dating to rock surfaces and boulders on the moraines and associated landforms to help define the timing of glaciation. We also applied OSL methods at one location within the Skardu Basin. Over the last decade, the application of the newly developing techniques of TCN surface exposure and OSL dating has allowed many of the Late Quaternary glacial successions within the Himalaya and Tibet to be dated with various degrees of confidence (Sharma and Owen, 1996; Richards et al., 2000a, b; Phillips et al., 2000; Owen et al., 2001, 2002a–c, 2003a, b, 2006; Tsukamoto et al., 2002; Finkel et al., 2003; Spencer and Owen, 2004; Seong et al., 2007a). We followed the methods and techniques in these studies as a framework for sampling and data analysis.

Samples for ^{10}Be TCN surface exposure dating were collected by chiseling ~500 g of rock from the upper surfaces of quartz-rich boulders along moraine crests or on glacially eroded bedrock surfaces. Locations were chosen where there was no apparent evidence of exhumation or slope instability. The largest boulders and the highest points on glacially eroded bedrock surfaces were chosen to help reduce the possibility that the boulders and rock surfaces may have been covered with snow for significant periods (several months of the year) or were previously covered with sediment. To provide a check on the reproducibility of the dating and a check for the possibility

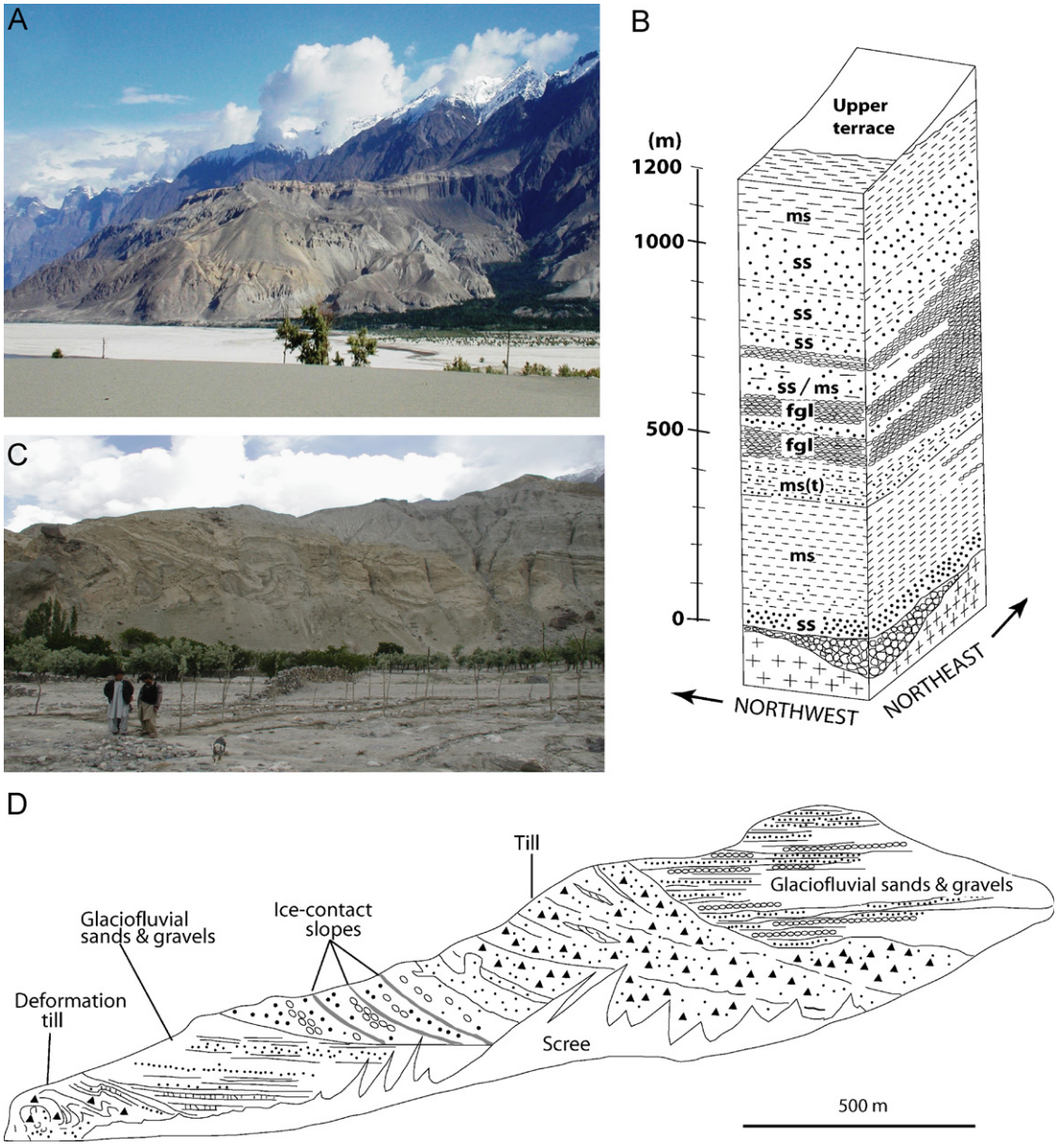

Fig. 2. The geomorphology of the Bunthang Sequence: (A) view of the Bunthang sequence near Skardu, looking northwest from the Karpochi Rock. The width of Bunthang outcrop in the view is ~5 km. The Indus River in the foreground flows from right to left. The vegetated area on the alluvial fan is the village of Kuardu. Pale horizontal stratified bed at top of the outcrop comprises interfingering glaciofluvial and lacustrine sediments, which overlie darker alluvial gravel deposit. The alluvial gravel units thin toward the Indus River; (B) schematic summary of the physical stratigraphy of the Bunthang Sequence (after Cronin et al., 1989). Lithologic abbreviations: ms is mudstone; ms (*t*) is rhythmically bedded mudstone; ss is sandstone; fgl is fanglomerate; (C) wet-sediment deformation structure developed within the Bunthang sequence. View looking south from the village of Kuardu; (D) modified version of Owen and Derbyshire's (1988) log showing the structures in the lower part of the Bunthang sequence viewed south from the village of Kuardu (35°24.087′N, 75°31.576′E).

of the inheritance of TCNs by prior exposure to cosmic rays, several (four to seven) samples from each moraine ridge or glacially eroded bedrock surface were sampled and dated. The degree of weathering and site conditions for each sampling site were recorded. Topographic shielding was determined by measuring the inclination from each sampling site to the top of surrounding mountain ridges and peaks.

All the samples for ^{10}Be TCN surface exposure dating were prepared in the geochronology laboratories at the University of Cincinnati. First, the samples were crushed and sieved. Quartz was then separated from the 250–500 μm particle size fractions using the methods of Kohl and Nishiizumi (1992). After the addition of ^{9}Be carrier (~0.07 mg/g of SiO_2), Be was separated and purified by ion exchange chromatography and precipitated at pH > 7. The hydroxides were oxidized by ignition in quartz crucibles. BeO was mixed with Nb metal and loaded into stainless steel cathodes for the determination of the ^{10}Be/^{9}Be ratios by accelerator mass spectrometry (AMS) at the Center for AMS in the Lawrence Livermore

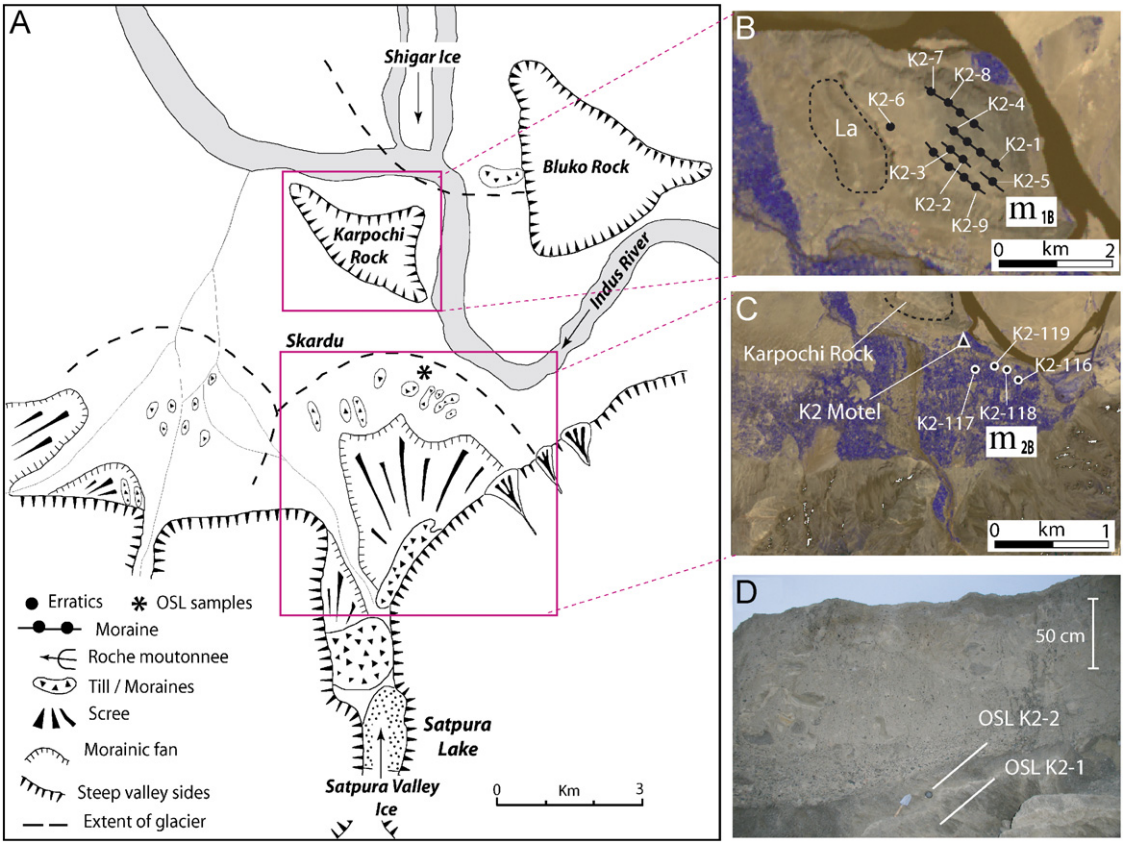

Fig. 3. Glaciated rock surfaces and glacial landforms around the Skardu: (A) map showing the extent of glacial ice in the Skardu area (after Owen, 1988); (B) ASTER image of moraine ridges, showing the locations where glacial boulders were sampled for ^{10}Be TCN exposure dating on the Karpochi Rock (each number refers to the number of the TCN sample). Stratified lake sediments (La) are present against the cliff of the Karpochi Rock; (C) ASTER image showing the locations of sampling sites used to define the ages of moraine near the K2 motel. Vegetation is highlighted in purple. m_{1B} and m_{2B} are moraine stratigraphy used in Table 2; (D) locations for OSL samples OSL K2-1 and OSL K2-2.

National Laboratory. Isotope ratios were compared to ICN Pharmaceutical, Incorporated ^{10}Be standards prepared by K. Nishiizumi (pers. comm., 1995), using a ^{10}Be half-life of 1.5×10^6 yr. The measured isotope ratios were corrected using blank samples (with a mean ^{10}Be/^{9}Be ratio of $1.5 \times 10^{-14} \pm 0.3 \times 10^{-15}$) and converted to TCN concentrations in quartz using the total ^{10}Be in the samples and the sample weights. TCN ^{10}Be concentrations were then converted to zero-erosion exposure ages using sea level high latitude (SLHL) ^{10}Be production rate of 4.98 atom/g of quartz/a (Stone, 2000; Balco and Stone, 2007). ^{10}Be production rates were scaled to the latitude and elevation of the sampling sites using the scaling factors of Stone (2000) with 3% SLHL muon contribution. There is still debate concerning the correct scaling method and SLHL rate, possibly impacting the model exposure age. However, uncertainties in absolute production rates and scaling factors have far less impact on relative chronologies for events in a limited geographic area.

Two sediment samples were collected for OSL dating from a terrace section in Skardu by hammering light-tight tubes into freshly exposed sediments (Fig. 3D). The tubes remained sealed until processed in the safe light conditions in the Geochronology Laboratory at the University of Cincinnati. Sample preparation follows the methods described in Owen et al. (2007). Approximately 20 g of the dried sub-sample from the sediment sample was ground to a fine powder and sent to the USGS Reactor in Denver for neutron-activation analysis (INAA) to determine the concentration of radioisotopes for dose-rate determination. Variable water content throughout the section may have occurred throughout the history of the section. However, it is not possible to determine the degree of such changes. The dose rate was therefore assumed to have remained constant and a $10 \pm 5\%$ water content value was used to help account for possible changes in water content.

Luminescence measurements were undertaken on quartz for the dominant particle size for each sample using a Riso Automated TL/IRSL/Blue DA-15 C/D OSL Dating System. Luminescence from the quartz grains was stimulated using an array of blue light emitting diodes (470 nm, 50 mW/cm^2) filtered using a green long-pass GG-420 filter. Detection was through a Hoya U-340 filter. All quartz aliquots were screened for feldspar contamination using infrared stimulation with infrared light emitting diodes (870 nm, 150 mW/cm^2). All OSL signals were detected using a 52 mm diameter photomultiplier tube (9235B). Riso *Sequence Editor* software was used for hardware control.

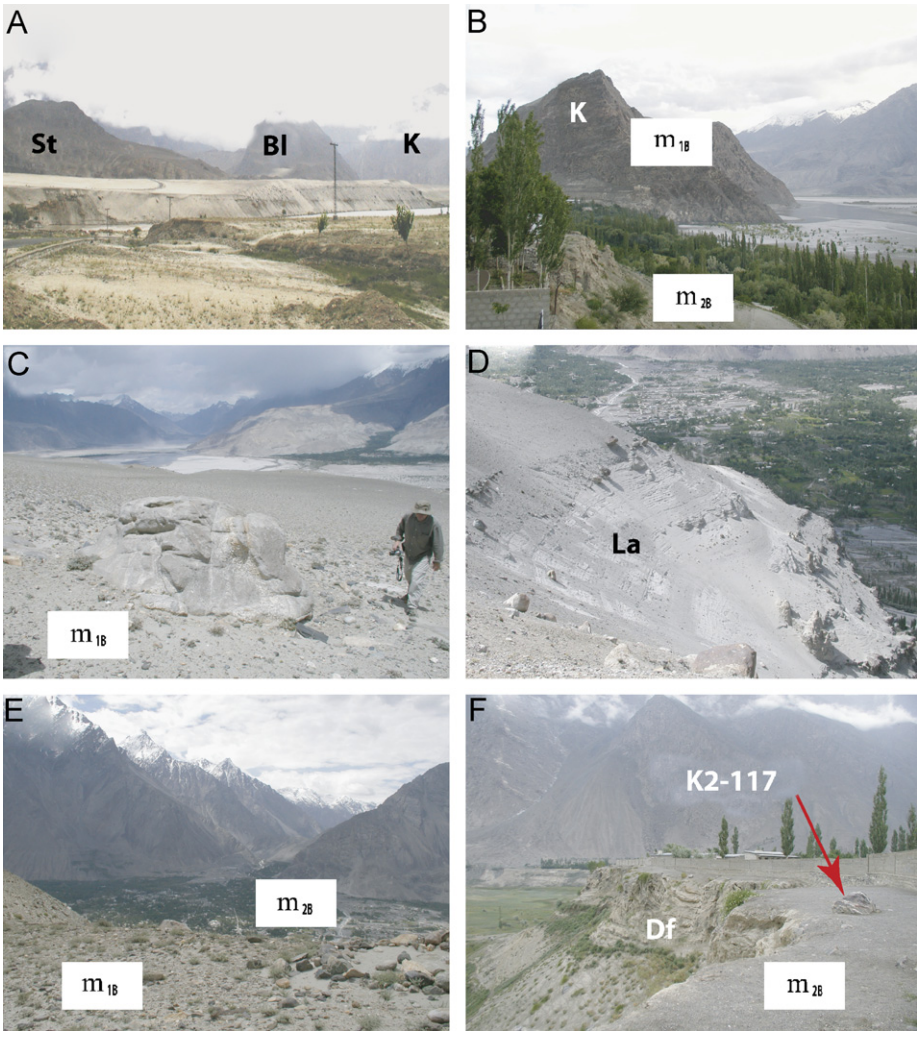

Fig. 4. Views of the geomorphology of the Skardu area; (A) glacially eroded mesas looking south (K—the Karpochi Rock; Bl—Bluko Rock; and St—Strondoka Ridge); (B) the Karpochi Rock from the K2 motel that is built on the alluvial fan produced during the Askole glacial stage; (C) a boulder (K2-6) looking south on top of the Karpochi Rock, which was sampled for TCN surface exposure dating; (D) stratified lake sediments (La) that are present against the cliff of the Karpochi Rock; (E) view looking south into the town of Skardu from the Satpura valley; (F) view looking southeast at the wet-sediment deformation structure overlain by glacial deposits formed by a tributary valley glacier advance during the Askole glacial stage. K2-117 was sample number for TCN exposure dating.

Equivalent dose (D_E) measurements were determined on multiple aliquots for each sample using the single aliquot regenerative (SAR) method protocol developed by Murray and Wintle (2000). The D_E value for every aliquot of each sample was examined using Riso *Analysis 3.22b* software. Aliquots with poor recuperation ($>10\%$) were not used in the age calculations. In fluvial sediments, a large spread of D_E values may reflect partial bleaching of sediment (Olley et al., 1999). To assess this problem, the D_E values for each sample were plotted on radial and probability distribution plots using the methods of Olley et al. (1999) and Wallinga (2002).

5. Sampled areas

The nine detailed study areas that were examined are outlined in this section.

5.1. Komara (area A)

The Bunthang Sequence of Cronin et al. (1989) was examined near the village of Komara (Fig. 2). At this location, basal till is dark gray with patchy brown oxidized areas. It is texturally very coarse, unstratified, and contains matrix-supported boulders up to several meters in diameter. The till overlies the bedrock (Fig. 2B). The till and associated sediments are deformed into folds (Fig. 2C). Similar deformation structures are present throughout the Skardu basin and for a considerable distance along the Shigar valley within younger sediments (Burgisser et al., 1982; Cronin et al., 1989). Owen (1988) explained the wet-sediment deformation of the Skardu fluvial and lacustrine beds by glaciotectonic deformation resulting from tributary valley glaciers advancing over wet and probably frozen sediments during glacial times.

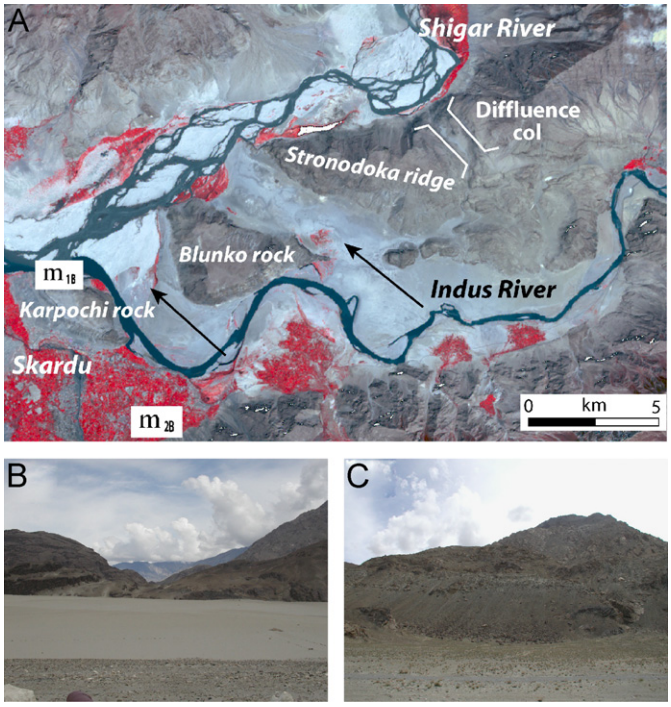

Fig. 5. Geomorphology of the Skardu basin and the diffluence col in the Shigar valley: (A) ASTER image of the Skardu basin, showing the diffluence col; (B) view of diffluence col looking northeast from the Shigar Valley; (C) Till within the diffluence col at 35°21.824′N, 75°44.393′E looking north.

Table 1
Correlations of the moraines between the valleys of the study regions A to I

Age	A	B	C	D	E	F	G	H	I	Glacial Stage
LIA								m_{1H}		Askole
4.4 ka		m_{3B}								Askole
5.7 ka							m_{2G}			Askole
									m_{3I}	
13–11 ka				m_{1D}	m_{1E}	m_{1F}	m_{1G}		m_{2I}	Mungo
									m_{1I}	
16 ka			m_{2C}							Mungo
			m_{1C}							
Penultimate glacial cycle or older		m_{1B}								Skardu
≫0.72 Ma	m1A									Bunthang

5.2. Skardu (area B)

The glacial surfaces described by previous workers (Drew, 1873; Dianelli, 1922; Cronin et al, 1989) were reassessed in the Skardu Basin and the Shigar valley are shown in Figs. 1B, 3–5. Two locations in the Skardu area were examined in detail. The first of these locations was Karpochi Rock, which is located at the confluence of the Indus and the Shigar Rivers and rises > 500 m above the present river bed (Fig. 4A). At least five NW-trending moraine ridges, parallel to the present Shigar River are present on top of the Karpochi Rock. Boulders up to 3 m in diameter are scattered on the crests of these moraines. The boulders comprise mainly granite and gneiss, and exhibit granular and cavernous weathering, and some are weathered level to the surface of the moraine (Fig. 4C). Nine samples (K2-1–K2-9) for TCN dating were collected from these moraines (Fig. 3A and B).

The second location comprises numerous hummocks that rise a few tens of meters above the present level of the Indus River, near the K2 Motel on the northeastern outskirts of Skardu (38°44.252′N, 75°16.365′E). These hummocks consist mainly of scattered boulders in association with sands and silts that are complexly folded and faulted (Figs. 1B, 3C). These landforms and their associated deformed sediments were described in detail by Owen (1988). He attributed their formation to glaciotectonism resulting from a glacier that advanced down the Satpura valley into the main Indus valley, which deposited moraines and deformed the fluvial and lacustrine sediments over which they advanced. Hewitt (1999) reinterpreted these hummocky landforms as a rock-avalanche deposit that he believed was produced by a bedrock failure on the east side of the lower Satpura valley, which he called the Satpura Lake–Skardu rock avalanche. However, Hewitt (1999) did not explain the complex deformation structures in the fluvial–lacustrine terraces at Skardu that were within his assigned limit of the rock avalanche. Similar structures also occur within the terraces at other locations outside of the rock avalanche limit (e.g., at the Indus bridge on the Skardu–Shigar road, 35°18′N/75°45′E). We therefore favor the interpretation of Owen (1988) and argue that the hummocks are moraines and that the terrace sediments have been glaciotectonized. Unfortunately, much of the moraine surface has been disturbed by grazing cattle and construction. Four samples (K2-116–K2-119) for TCN surface exposure age dating, however, were collected from the best-preserved moraine. Two samples for OSL dating (OSL K2-1 and OSL K2-2) were collected from fluvial sands beneath a diamict (interpreted as a till) in the deformed terraces that are associated with the moraines beneath the K2 Motel (Fig. 3D).

An impressive diffluence col is present on the north side of Stronodoka ridge, one of the glacially eroded mesas (Fig. 5). This location has the glacially eroded surfaces along the valley floor and pale-colored till on a surface 150 m high above the valley floor. No samples were collected from this location because there were no quartz-rich lithologies present for ^{10}Be TCN surface exposure dating.

5.3. Mungo (area C)

One of the best-preserved glacial benches is present near the confluence of the Shigar and Braldu Rivers near the village of Mungo (Figs. 1C and 6). This surface rises 500 to 1500 m above the present river bed and comprises three

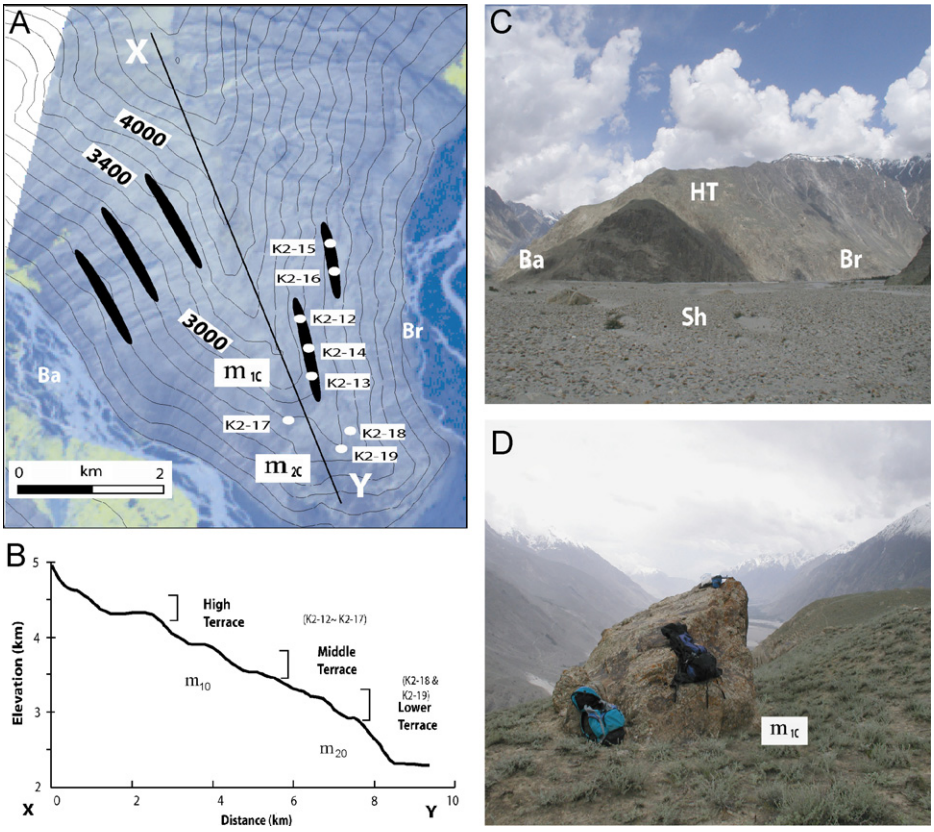

Fig. 6. Views showing the glacial landforms formed near Mungo; (A) Mungo terraces formed by a thick valley glacier during the Mungo glacial stage and view of moraine ridges and sampling locations for TCN surface exposure dating. Braldu River and Basha River confluence into Shigar River south of the Mungo terrace; (B) longitudinal profile of Mungo terraces; (C) view of Mungo terraces looking northwest. HT represents high terrace that is a bench located at the altitude of between 4000 and 4500 m asl; (D) view of a glacial erratic (K2-16) on the middle terrace looking south. The Shigar River is in the background.

minor surfaces at 2800–3000, 3400–3800, 4200–4500 m asl. Moraine ridges are present on each bench and trend NNE to SSW, approximately parallel to the course of the Shigar valley (Fig. 6). The moraine ridges are subdued, but had abundant boulders on them. The boulders are highly weathered and some of them have weathering pits that are as much as 10 cm deep. Lichens reaching several centimeters in diameter are abundant on the boulders. Eight boulders (K2-12–K2-19) were sampled for TCN surface exposure dating from the middle (K2-12–K2-17) and lower (K2-18 and K2-19) surfaces.

5.4. Dassu (area D)

Glacially eroded bedrock surfaces and roche moutonnées rise from 80 m to several hundred meters above the present Shigar River at Dassu (Figs. 1D and 7). Glacial striations are abundant on these surfaces. The valley sides have irregular rock hummocks that are 5–7 m long and 2–3 m high (Fig. 7D). Below the glacial eroded surfaces the valley is dominantly V-shaped (Fig. 7C). Fluvially eroded and polished strath terraces rise 20–30 m above the present river bed, ~60 m lower than the glacially eroded surfaces. Four samples (K2-23–K2-26) for TCN surface exposure dating were collected from the glacially eroded bedrock surface.

5.5. Chakpo (area E)

Impressive glacially eroded bedrock and glacial benches occur south of the village of Chakpo and rise 200–500 m above the present river bed (Figs. 1E and 8). Deep fresh striations, and boulders and erratics are present on these glaciated surfaces (Fig. 8B). At this location the Braldu valley is much narrower than further downstream. The valley continues to broaden and deepen upstream towards the contemporary snout of the Biafo and Baltoro Glacier. The surface on the opposite side of the valley was deeply excavated by a landslide failure. Five samples (K2-31–K2-33) were collected for TCN surface exposure dating at this location.

5.6. Pakora (area F)

Impressive glacially eroded bedrock surfaces and roche moutonnées are present near Pakora, located ~20 km upstream from Chakpo (Figs. 1F and 9). These have deep (several mm) and fresh striations on their surfaces that

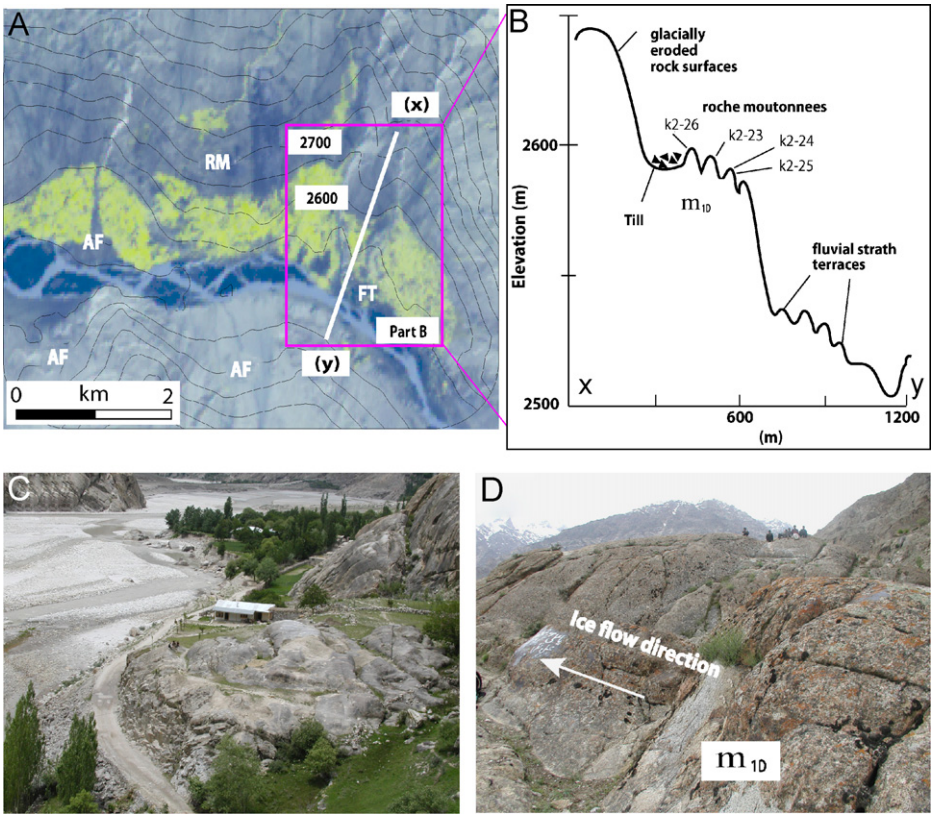

Fig. 7. Glacial landforms around Dassu: (A) ASTER image of area around Dassu village, showing alluvial fans (AF), fluvial terraces (FT), and roche moutonnée (RM); (B) cross valley profile showing the main landforms: (C) view of fluvial strath terrace around Dassu Motel. Braldu River is toward the top of the photography; (D) exposure of glacially eroded rock surface above Dassu. The children on the top is for scale and glacier advanced from right to left.

trend E-W, which are approximately parallel to the present Braldu valley (Fig. 9B). On average, the glacially eroded slope rises >100 m above the valley and slopes between 15° and 20°. Four samples (K2-62–K2-63) were collected for TCN surface exposure dating at this location.

5.7. Askole (area G)

Glacially eroded bedrock is present south of the village of Askole, ~20 km from the terminus of the Biafo glacier (Figs. 1G, 10 and 11). Roche moutonnées are more developed on the south side of the valley and rise hundreds of meters above the present river bed (Fig. 10B). The bedrock surface has undulating hummocks 6–8 m long and 1–2 m deep. The striations are fresh and are several mm deep. Till is present just beyond the lowest glacially polished surface and glaciofluvial sediments are present on a glacially eroded surface at 40–80 m above the present Braldu River. Twelve samples (K2-48–K2-59) were collected for TCN surface exposure dating to define the age of the glacially polished surfaces at different elevations from 3630 to 3880 m asl in this study area.

An impressive lateral moraine occurs several hundred meters above the Braldu river valley near Askole (Fig. 10C). It is very subdued and scattered boulders on its surface comprise granites and metasedimentary rocks. These boulders are weathered with pits as much as 5 cm deep. Abundant lichens cover the boulders. Six samples (K2-65–K2-70) were collected for TCN surface exposure dating at this location.

5.8. Biafo (area H)

Sharp-crested and well-formed latero-frontal moraines are present within tens of meters of the contemporary snout of the Biafo glacier (Figs. 1H and 12). The moraine ridges are several meters high and comprise boulders that reach several meters in diameter. The boulders are angular and fresh with little of evidence of weathering. A roche moutonnée is present near the porters' latrines directly below the snout of the Biafo glacier. Seven samples (K2-90–K2-96) were collected from quartz-rich boulders on the outermost moraine ridge to define the age of the youngest advance of the Biafo glacier (Fig. 12).

5.9. Biafo–Panmah (area I)

Glacial benches exist up to 1000 m above the valley floor on the northern slope of the Braldu valley between the Biafo and Panmah Glaciers (Figs. 1I and 13). These comprise three main surfaces, at 3200–3300, 3600–3800 and 4000–4300 m asl. The highest and middle benches

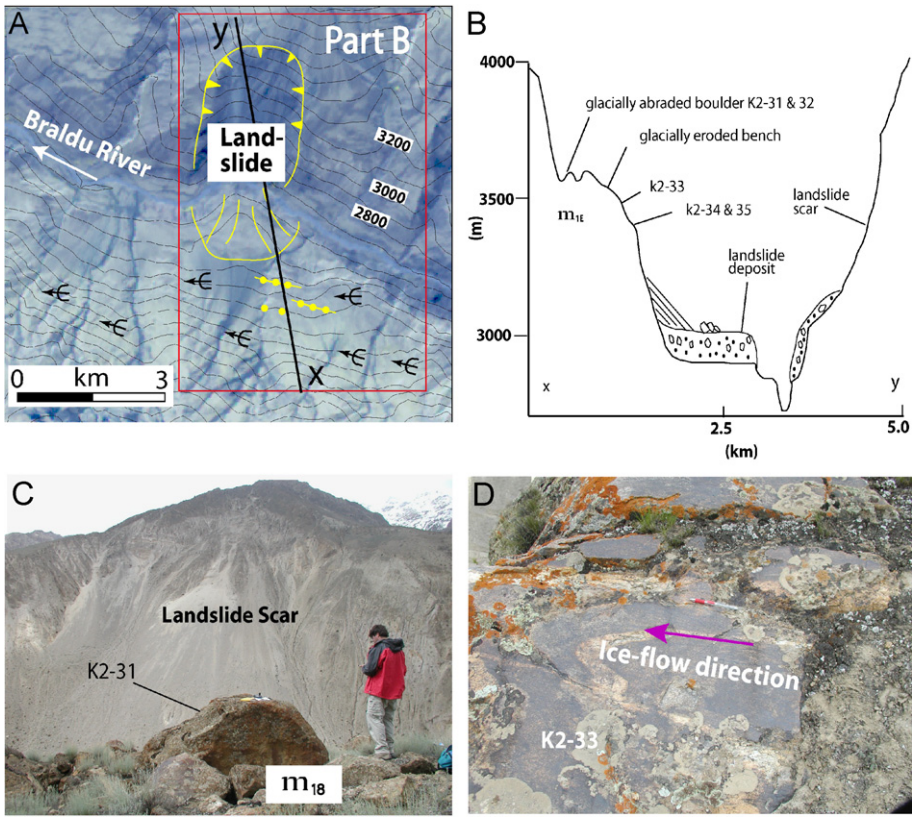

Fig. 8. The geomorphology around Chakpo: (A) ASTER image showing a small portion of the much larger Gomboro landslide and locations of glacial landforms for TCN surface exposure dating. The arrows indicate the positions of roche moutonnées. See Fig. 3 for the legend; (B) illustration of geomorphology and sampling sites around Chakpo. The landslide map is diagrammatic of a larger whole. Hewitt (1998) named this landslide the Gomboro Complex I; (C) view of landslide scar and boulder erratic (K2-31) looking north; (D) exposure of glacier eroded and polished surface for sampling (K2-33). The landslide shown in photos A, B and C was dated by Shroder et al. (2007) to the Lateglacial.

comprise ice-polished surfaces with moraine ridges, whereas the lower bench comprises mainly subglacial till containing boulders. All the boulders on the upper two benches are highly weathered and most of them have weathering pits reaching up to 10 cm deep and have similar weathering characteristics. Boulders in the till of the lower bench are less weathered, with only 1–2 cm-thick patchy areas of surface exfoliation. The moraine ridges trend east, parallel to the present Braldu River. To define the age of the surfaces, eight samples (K2-72–K2-79) were collected from the upper surface, six samples (K2-82–K2-85) from the middle surface, and four samples (K2-86–K2-89) from the lower surface for TCN surface exposure dating.

6. Dating results

The moraines and associated landforms in each study area are listed in Tables 1 and 2, and assigned to an appropriate glacial stage. The TCN dating defines the timing of three of these glacial stages. The TCN ages determined for each study area are shown in Fig. 14. The ages for each glacial stage are summarized in the following sections. However, it was not possible to define the absolute ages of the oldest glacial stage, the Bunthang glacial stage, because there were no boulders suitable for TCN surface exposure dating.

The concentrations of ^{10}Be TCN that were measured (Table 2) allowed model surface exposure ages to be calculated for each sample. The very young TCN dates (several hundred years; Figs. 1H and 12) and the lack of old dates for boulders on the youngest moraines suggest that inheritance of TCNs in glacial boulders is low (probably a few hundred years or less) in this region. This is to be expected in such a dynamically eroding environment where fresh rock is being continuously supplied to glacier surfaces by rock falls and avalanching. In addition, the tight clustering of TCN surface exposure ages for multiple samples collected on individual surfaces provides confidence in the TCN surface-exposure dating method. The exception, however, is the oldest surface m_{1B} where there is a large spread of ages (Figs. 3B and 14). Given the stochastic nature of weathering processes, a large spread of TCN surface exposure ages for the older deposits is not surprising, but the tight clustering of TCN surface exposure ages for the younger landforms provides confidence in the dating. For each of the study areas, the TCN surface exposure ages on sampled moraines confirm the morphostratigraphic relationship: that is, each set of dates on each morphostratigraphically younger moraine are

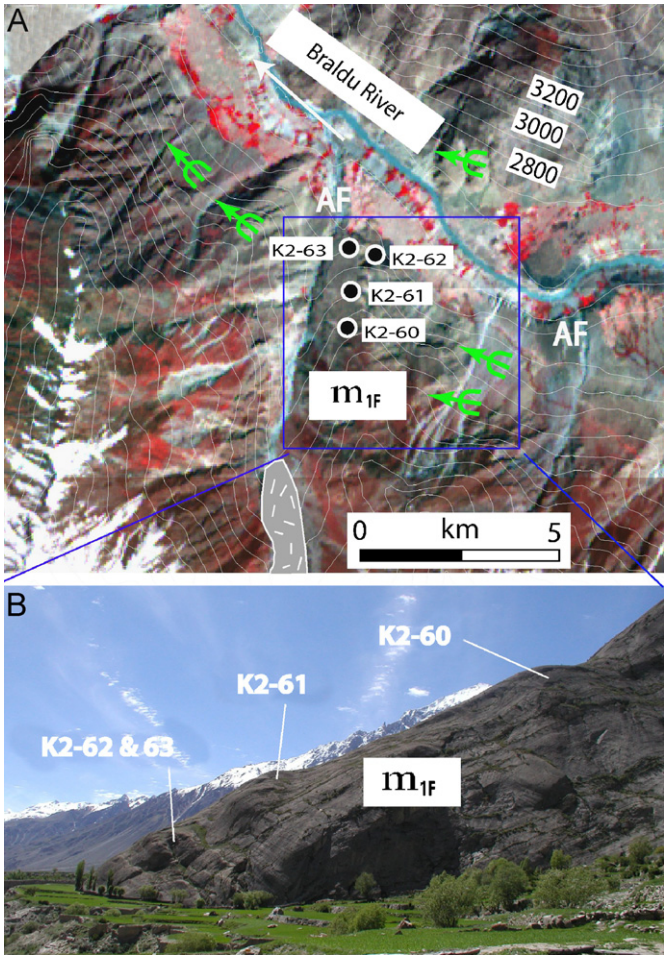

Fig. 9. The geomorphology of the Pakora area: (A) ASTER image showing roche moutonnées (green arrows) and associated landforms. See Fig. 3 for the legend; (B) view looking west of roche moutonnée that was sampled for TCN surface exposure dating.

progressively younger. All the TCN ages should be considered as minimum ages because of the uncertain effects of weathering, erosion and snow cover.

The TCN ages with zero erosion are used because it is not possible to determine the erosion rates for each boulder or bedrock surface. However, erosion rates can be estimated using the oldest boulder age (K2-1–K2-9) and applying Lal's (1991) methods. This gives a boulder erosion rate of between ~3 and 7 m/Ma. Given that these are likely maximum boulder erosion rates and if the boulders are considered to be in steady-state erosional equilibrium, a reasonable boulder erosion rate for the region is estimated to be ~3 m/Ma. This rate is similar to rates derived from TCN data for the adjacent regions (Lal et al., 2003; Owen et al., 2006; Seong et al., 2007a) and other semi-arid regions outside of the Tibetan–Himalayan orogen (e.g. Small et al., 1997; Zehfuss et al., 2001: Owen et al. 2007). Assuming that all the boulders and glacially eroded bedrock surfaces that were sampled weather at the rate of 3 m/Ma, an age of 10 ka calculated assuming zero boulder erosion would underestimate the true age by 3%; an age of 50 ka, by 9%; an age of 100 ka, by 28%.

The OSL dating results for quartz extracted from the sediment samples are summarized in Table 3. The dose rates are well within the normal range of values expected for fluvial sediments. All aliquots produced luminescence signals that were >10 times background levels. Both samples showed some evidence for partial bleaching, with ~10–20% of the aliquots outside the normally distributed population. Both samples have mid-Holocene ages.

6.1. Bunthang glacial stage

The Bunthang basal till is overlain by 1.3 km thick succession of fluvial/glaciofluvial, lacustrine, and alluvial sediments (Cronin, 1989; Cronin et al., 1989; Fig. 2B). Owen and Derbyshire (1988) interpreted the Bunthang sequence as a succession of sediments that had undergone glaciotectonic deformation. Re-examination of these sediments confirms that the basal till was deformed by glaciotectonic processes. The apparent discontinuities throughout the overlaying sediments were interpreted by Owen and Derbyshire (1988) to be faults. However, these discontinuities are more likely to be ice-contact depositional surfaces down which sediment was deposited from a large glacier that filled the Indus valley at this location (Fig. 2D). These are similar in form to those described by Benn and Owen (2002). Cronin (1989) and Cronin et al. (1989) showed that the basal till is predominantly reversely magnetized, implying the thick, extensive glacier occupied the Indus Valley during the Matuyama chron, between 3.2 and 0.72 Ma. However, since this till is deformed and in places is inverted, the validity of the reversed magnetism might be questionable.

6.2. Skardu glacial stage

The valley glaciers during this stage advanced and formed a glacial system that extended >150 km beyond the present Baltoro glacier. Well-preserved moraines of this glacial stage are present on the glacially eroded mesa, Karpochi Rock, which rises >500 m from the present Indus River bed (m_{1B} in Figs. 3 and 4).

The data show that the boulders on the Skardu glacial stage moraines range in age from 70 to 170 ka, suggesting that this moraine is of great antiquity. Most of the boulders on this moraine were intensively weathered and therefore these ^{10}Be TCN ages must be considered to be truly minimum ages. The youngest age (K2-9 ca 70 ka) is from a weathered and low-lying boulder that is probably the most weathered of this set. Although there is a noticeable spread of ages, which suggests the youngest ages represent significant erosion and/or exhumation of boulders, this landform could be broadly assigned to a glaciation that occurred during the penultimate glacial cycle. However, it could be significantly older, formed during an earlier glacial cycle. Moreover, given a likely boulder and glacially eroded bedrock weathering rate of 3 m/Ma, the ages of the boulders probably range from ~84 to 235 ka and therefore

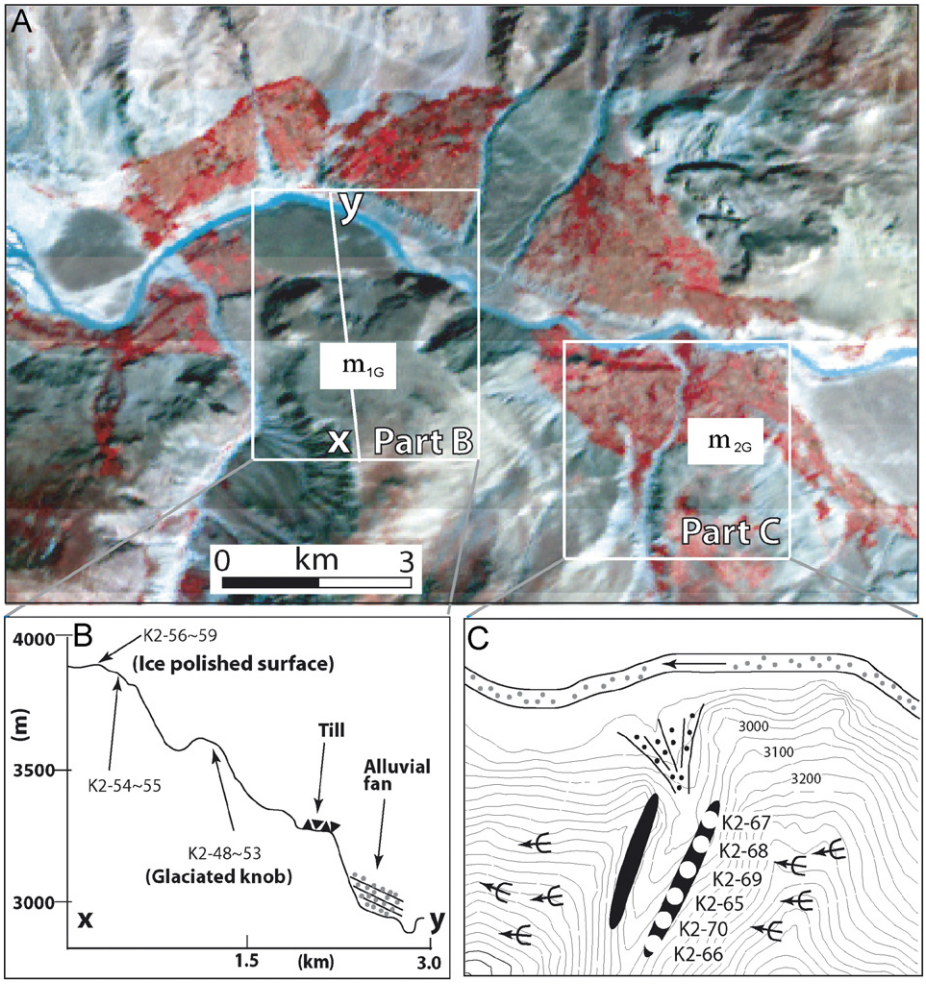

Fig. 10. The geomorphology of the Askole region: (A) ASTER image showing the two study sites around Askole. The moraines labeled m_{1G} and m_{2G} were formed during the Mungo and Askole glacial stage, respectively; (B) cross valley profile showing the main landforms formed during the Mungo glacial stage; (C) geomorphic map of southern side of Askole. See Fig. 3 for the legend.

this glacial stage might be assigned to marine Oxygen Isotope Stage (MIS) 6, but is likely to be considerably older.

6.3. *Mungo glacial stage*

Evidence for glacial advances during this stage is recognized in six different areas (Mungo, Dassu, Chakpo, Pakora, Askole, and Biafo–Panmah). These are highlighted within the purple boxes in Fig. 1. Fig. 15 shows the ages and relative positions of the glacier landforms that were dated for the Mungo glacier stage and schematic glacier profiles are presented to allow an examination of the relative heights of each landform. The tight clustering of boulder ages on the moraines suggests that the glaciers were present at these locations between ~16 and ~11 ka (Fig. 14). The ^{10}Be TCN surface exposure ages for each set of data were converted to a probability distribution and summed to show the relative strengths of the TCN surface exposure ages of each advance (Fig. 14). Shroder et al. (2007) and Seong et al. (2007b) provide additional TCN surface exposure ages on landslides and strath terraces in the Shigar and Braldu valleys.

The TCN surface exposure ages for the two sets of latero-frontal moraines at Mungo range between 14.6 and 16.7 ka, with tight clustering at about 16.3 ka (Figs. 1C and 6). The youngest age (14.6 ka from K2-19) is likely due to post-depositional weathering and/or toppling. The moraines at Mungo are at altitudes ranging from 2800 to 3800 m asl. This shows that the extensive valley glacier that produced them was at least 1 km thick at this location and advanced to Mungo and into the Shigar valley at ~ 16 ka, ~80 km from the snout of the contemporary Baltoro glacier. However, it is not possible to assess how long the glacier existed in the Braldu and Shigar valleys and whether these TCN ages might represent the final stages of a glacial advance that started much earlier in MIS 2 and was broadly synchronous with the global Last Glacial Maximum (gLGM). Similar Lateglacial ages are derived from boulders collected from the high glacial benches at the Biafo–Panmah study site. The difference in height between the moraines (ranging from 3440–4225 m asl) at this site is

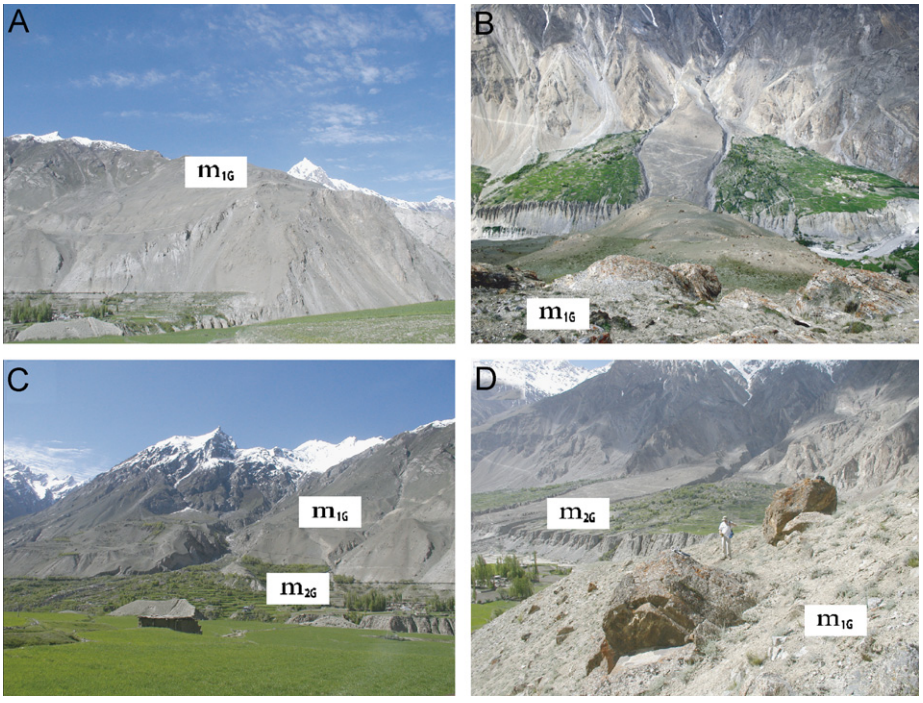

Fig. 11. Views of glacial landforms around the village of Askole: (A) view looking south from Askole at glacial deposits (m_{1G}) produced during the Mungo glacial stage; (B) view looking north at subdued moraines of m_{1G} and scattered glacial boulders; (C) view looking southeast from Askole base camp at glacial landforms produced during the Mungo glacial stage (m_{1G}) and the Askole glacial stage (m_{2G}), respectively; (D) view looking northwest across a lateral moraine (m_{1G}) that formed during the Askole glacial stage.

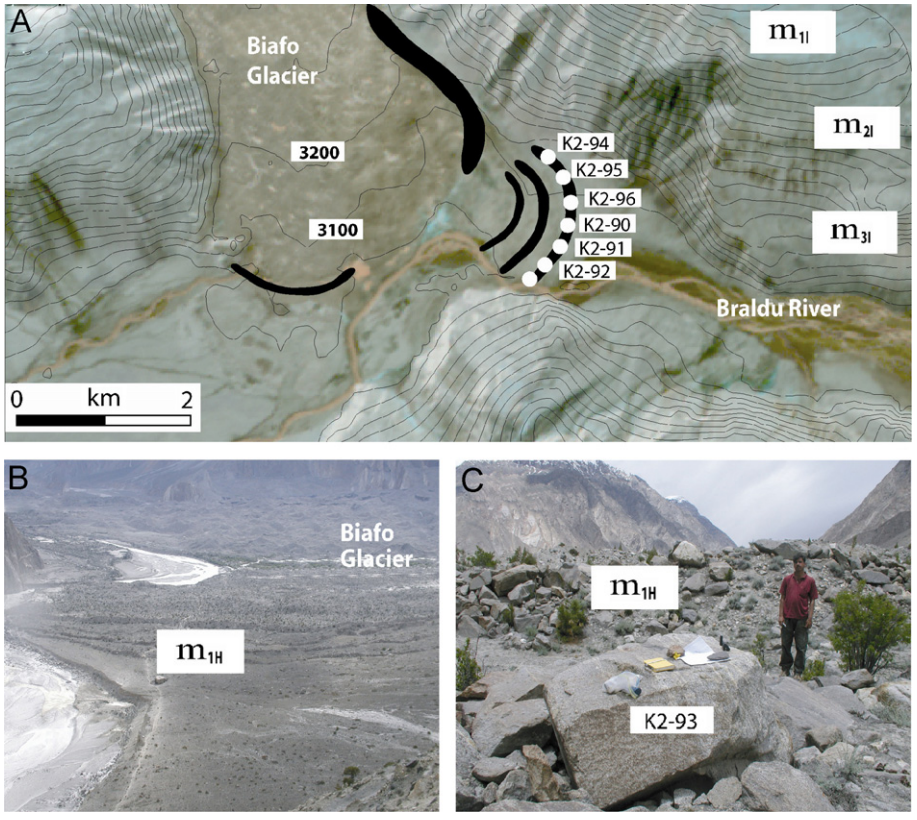

Fig. 12. Views illustrating the successive latero-frontal moraines at the Biafo Glacier: (A) ASTER image of the terminus of Biafo Glacier with sampling locations of boulders for TCN surface exposure dating; (B) view of multiple latero-frontal moraines developed around the Biafo Glacier looking east from high surface between the Biafo and Panmah Glacier; (C) a boulder (K2-93) on the most outer moraine for TCN surface exposure dating.

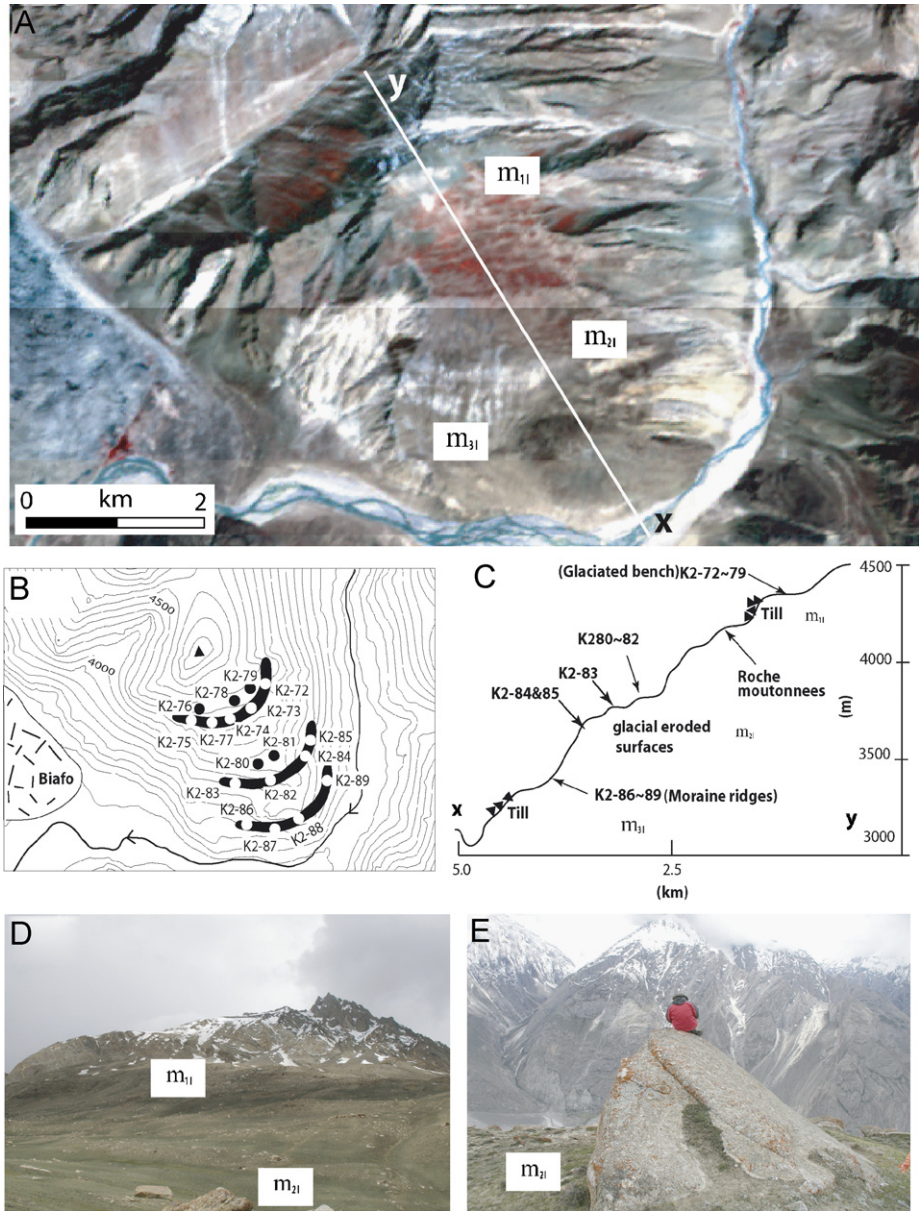

Fig. 13. The glacial landforms between the Biafo and Panmah Glaciers: (A) ASTER image of glacially eroded surfaces; (B) locations of moraine ridges and boulders for TCN surface exposure dating. Numbers on the map refer to sampling number; (C) cross-valley profile showing the main glacial landforms; (D) view looking north up the surface at 4000–4500 m asl from the glaciated middle surface (m_{2I}). m_{1I} and m_{2I} indicate the high surface and middle surface, respectively; (E) view of a boulder on the middle surface, which consists mainly of a moraine ridge and subglacial landform.

at least 800 m, again supporting the view of that the valley glacier was very thick.

Five locations in Braldu valley have glacial landforms that date to between 11 and 13 ka (Figs. 14 and 15). The ages for the bedrock surfaces at Dassu range from ~12 to 13 ka. At Chakpo the TCN ages range from 11 to 1 ka. The youngest boulder age (K2-32 at 1.2 ± 0.2 ka) is probably the result of post-glacial toppling or exhumation due to the removal of surface material. This is not plotted in Fig. 14.

These two sets of ages contrast with the TCN ages obtained by Shroder et al. (2007) for a large landslide (the Gomboro rockslide) near Chakpo, which has ages ranging from 12.6 to 14.6 ka and overlies the glacial landforms. The slightly older ages on the Gomboro rockslide can be explained by inheritance of TCNs in the rockslide boulders if they had been exposed to cosmic rays prior to deposition. This is likely because the samples collected were from an area of near the front of the rockslide and were likely carried down on mass preserving the relative stratigraphy and the bedrock surface of the exposed bedrock wall that failed. Alternatively, the younger ages on the glacial landforms might be a consequence of shielding of their surfaces due to sediment cover. It is noteworthy that the samples from Dassu and one of the samples from Chakpo were collected from very-well-preserved bedrock surfaces. The preservation of the surfaces might indicate that they were covered and protected by sediment for sometime after the glacier had retreated and hence they provide slightly

Table 2
Sampling locations for boulders, boulder size, topographic shielding factors, ^{10}Be concentrations, and ^{10}Be surface exposure ages

Sample ID	Latitude (±0.001N°)	Longitude (±0.001E°)	Altitude (m asl)	Shielding factor[a]	Boulder height/ width (m)	^{10}Be (10^6 atoms/g)[b]	^{10}Be Exposure age (ka)	Map location on Fig. 1	Moraine number
K2-1	35.315	75.626	2598	1.00	2.1/1.9	3.49±0.11	124.9±4.1	B	m_{1B}
K2-2	35.314	75.625	2601	1.00	3.2/2.5	4.65±0.07	167.6±2.5	B	m_{1B}
K2-3	35.314	75.625	2611	1.00	4.7/2.6	3.86±0.09	137.5±3.4	B	m_{1B}
K2-4	35.315	75.623	2598	1.00	1.1/2.8	4.71±0.09	170.2±3.4	B	m_{1B}
K2-5	35.314	75.626	2602	1.00	1.1/2.3	2.94±0.05	104.3±1.9	B	m_{1B}
K2-6	35.314	75.627	2613	1.00	1.4/5.1	4.02±0.11	143.2±4.0	B	m_{1B}
K2-7	35.317	75.621	2545	1.00	0.9/2.9	2.53±0.06	93.0±2.3	B	m_{1B}
K2-8	35.318	75.618	2557	1.00	1.2/2.6	3.10±0.07	113.5±2.8	B	m_{1B}
K2-9	35.318	75.617	2557	1.00	0.9/3.5	1.91±0.05	70.3±1.7	B	m_{1B}
K2-12	35.677	75.469	2950	1.00	1.0/3.6	0.58±0.01	16.1±0.4	C	m_{1C}
K2-13	35.677	75.469	2952	1.00	2.0/3.3	0.60±0.02	16.7±0.4	C	m_{1C}
K2-14	35.677	75.475	2945	1.00	0.6/1.5	0.58±0.02	16.1±0.5	C	m_{1C}
K2-15	35.679	75.469	2950	1.00	2.6/6.1	0.58±0.02	16.3±0.6	C	m_{1C}
K2-16	35.678	75.469	2951	1.00	0.6/1.2	0.58±0.02	16.0±0.4	C	m_{1C}
K2-17	35.676	75.469	2950	1.00	1.1/1.1	0.58±0.02	16.3±0.4	C	m_{1C}
K2-18	35.675	75.466	2868	1.00	1.0/1.4	0.56±0.01	16.4±0.4	C	m_{1C}
K2-19	35.675	75.466	2865	1.00	0.7/2.0	0.50±0.02	14.6±0.5	C	m_{1C}
K2-23	35.718	75.520	2646	0.96	Bedrock	0.37±0.01	12.9±0.5	D	m_{1D}
K2-24	35.718	75.520	2631	0.96	Bedrock	0.35±0.01	12.4±0.5	D	m_{1D}
K2-25	35.718	75.520	2631	0.96	Bedrock	0.34±0.01	12.1±0.4	D	m_{1D}
K2-26	35.719	75.520	2650	0.96	Bedrock	0.36±0.01	12.6±0.4	D	m_{1D}
K2-31	35.721	75.676	3164	0.94	1.6/10.4	0.40±0.01	10.4±0.3	E	m_{1E}
K2-32	35.722	75.674	3166	0.94	1.6/10.4	0.06±0.01	1.2±0.2	E	m_{1E}
K2-33	35.724	75.672	3052	0.96	Bedrock	0.39±0.01	10.7±0.4	E	m_{1E}
K2-34	35.672	75.799	3160	0.94	Bedrock	[c]		E	m_{1E}
K2-35	35.672	75.799	3164	0.94	Bedrock	[c]		E	m_{1E}
K2-48	35.671	75.799	3633	1.00	1.6/2.8	0.60±0.02	11.4±0.4	G	m_{1G}
K2-49	35.671	75.799	3631	1.00	0.8/2.5	0.61±0.02	11.4±0.4	G	m_{1G}
K2-50	35.671	75.799	3640	1.00	0.8/2.5	0.65±0.02	12.3±0.4	G	m_{1G}
K2-51	35.671	75.799	3644	1.00	2.0/4.7	0.60±0.02	11.3±0.3	G	m_{1G}
K2-52	35.667	75.798	3636	1.00	1.7/2.2	0.60±0.02	11.2±0.3	G	m_{1G}
K2-53	35.667	75.797	3643	1.00	3.9/5.2	0.65±0.02	12.1±0.3	G	m_{1G}
K2-54	35.666	75.797	3824	1.00	0.4/6.1	0.48±0.01	8.2±0.2	G	m_{1G}
K2-55	35.666	75.796	3825	1.00	2.3/2.9	0.71±0.02	12.1±0.3	G	m_{1G}
K2-56	35.668	75.797	3881	1.00	1.5/7.4	0.73±0.02	12.0±0.4	G	m_{1G}
K2-58	35.694	75.719	3879	1.00	1.0/2.4	0.72±0.03	11.8±0.4	G	m_{1G}
K2-59	35.694	75.719	3811	1.00	1.3/3.2	0.72±0.02	12.3±0.3	G	m_{1G}
K2-60	35.694	75.719	3031	0.94	Bedrock	0.41±0.01	11.4±0.3	F	m_{1F}
K2-61	35.694	75.718	3032	0.93	Bedrock	0.40±0.01	11.4±0.3	F	m_{1F}
K2-62	35.672	75.814	3017	0.94	Bedrock	0.38±0.02	10.9±0.4	F	m_{1F}
K2-63	35.672	75.814	2944	0.69	Bedrock	0.29±0.01	11.7±0.4	F	m_{1F}
K2-65	35.672	75.814	3113	0.80	2.5/3.5	0.40±0.01	12.6±0.4	G	m_{2G}
K2-66	35.672	75.814	3128	0.80	1.2/2.0	0.16±0.01	5.1±0.2	G	m_{2G}
K2-67	35.672	75.814	3122	0.80	1.5/1.7	0.17±0.01	5.4±0.2	G	m_{2G}
K2-68	35.672	75.814	3113	0.80	0.7/1.0	0.18±0.01	5.8±0.2	G	m_{2G}
K2-69	35.703	75.954	3109	0.80	1.4/0.9	0.21±0.01	6.5±0.2	G	m_{2G}
K2-70	35.703	75.952	3106	0.79	1.2/1.7	0.18±0.01	5.7±0.2	G	m_{2G}
K2-72	35.703	75.953	4209	1.00	0.9/3.4	0.91±0.02	12.7±0.3	I	m_{1I}
K2-73	35.704	75.952	4213	1.00	1.9/2.1	0.93±0.02	12.9±0.3	I	m_{1I}
K2-74	35.703	75.952	4212	1.00	1.1/2.8	0.94±0.02	13.1±0.3	I	m_{1I}
K2-75	35.703	75.948	4215	1.00	1.6/5.0	0.92±0.03	12.7±0.4	I	m_{1I}
K2-76	35.703	75.947	4211	1.00	1.0/3.1	1.19±0.03	16.5±0.4	I	m_{1I}
K2-77	35.703	75.943	4211	1.00	2.6/1.3	0.96±0.02	13.3±0.3	I	m_{1I}
K2-78	35.695	75.957	4225	1.00	1.7/4.1	0.94±0.02	13.0±0.3	I	m_{1I}
K2-79	35.694	75.958	4221	1.00	1.2/4.0	0.89±0.02	12.4±0.3	I	m_{1I}
K2-80	35.694	75.958	3823	0.81	1.0/3.9	0.71±0.02	15.0±0.4	I	m_{2I}
K2-81	35.693	75.960	3821	0.81	1.1/2.7	0.73±0.02	15.3±0.5	I	m_{2I}
K2-82	35.692	75.960	3818	0.81	2.0/1.8	0.70±0.02	14.7±0.4	I	m_{2I}
K2-83	35.692	75.961	3779	1.00	3.8/4.1	2.56±0.06	45.0±1.1	I	m_{2I}
K2-84	35.689	75.941	3768	1.00	1.9/4.7	0.68±0.02	11.9±0.3	I	m_{2I}
K2-85	35.689	75.941	3766	0.99	5.3/9.1	0.69±0.03	12.2±0.5	I	m_{2I}

Table 2 (*continued*)

Sample ID	Latitude (±0.001N°)	Longitude (±0.001E°)	Altitude (m asl)	Shielding factor[a]	Boulder height/ width (m)	^{10}Be (10^6 atoms/g)[b]	^{10}Be Exposure age (ka)	Map location on Fig. 1	Moraine number
K2-86	35.689	75.941	3445	0.98	1.0/2.7	0.51±0.01	11.0±0.3	I	m_{3I}
K2-87	35.689	75.941	3442	0.98	0.5/1.5	0.54±0.02	11.5±0.5	I	m_{3I}
K2-88	35.688	75.927	3447	0.98	0.6/1.4	0.58±0.02	12.3±0.3	I	m_{3I}
K2-89	35.688	75.927	3441	0.98	0.7/2.2	0.51±0.01	10.9±0.3	I	m_{3I}
K2-90	35.688	75.927	3095	0.97	1.2/1.9	0.02±0.00	0.4±0.1	H	m_{1H}
K2-91	35.695	75.927	3096	0.96	0.6/1.7	0.04±0.01	0.9±0.2	H	m_{1H}
K2-92	35.687	75.926	3094	0.96	0.7/0.9	0.03±0.00	0.8±0.1	H	m_{1H}
K2-93	35.686	75.926	3090	0.96	0.5/1.4	0.08±0.01	2.1±0.2	H	m_{1H}
K2-94	35.688	75.925	3096	0.96	0.8/2.0	0.04±0.01	0.9±0.2	H	m_{1H}
K2-95	35.292	75.662	3087	0.96	1.2/1.7	0.02±0.00	0.4±0.1	H	m_{1H}
K2-96	35.292	75.662	3116	0.97	1.4/2.2	0.05±0.01	1.2±0.1	H	m_{1H}
K2-116	35.292	75.662	2276	1.00	3.2/2.5	0.12±0.02	5.3±0.7	B	m_{2B}
K2-117	35.292	75.662	2276	1.00	2.7/2.2	0.09±0.00	3.7±0.2	B	m_{2B}
K2-118	35.315	75.626	2276	1.00	2.8/3.1	0.11±0.00	4.6±0.2	B	m_{2B}
K2-119	35.314	75.625	2276	1.00	3.5/2.9	0.09±0.00	3.9±0.2	B	m_{2B}

Note: Minimum ^{10}Be TCN ages were calculated using Stone (2000) scaling factors; sea-level high-latitude (SLHL) production rate = 4.98 ^{10}Be atoms/g quartz/year; zero erosion rate; and sample thickness of 5 cm; asl—above sea level. Uncertainties include analytic errors (weighing of sample, weighing and concentration of spike, and AMS error) and attenuation length. Uncertainties related to production rate and scaling factors were not explicitly treated here.

[a]Shielding factor as calculated to correct for topographic barriers using the methods of Nishiizumi et al. (1989).

[b]Atoms of ^{10}Be/g of quartz before application of shielding correction factor.

[c]^{10}Be concentrations were too low to be measured.

younger ages than the true age for glacier retreat. Despite the small conflict in ages between the glacial landforms and the rockslide, the strong clustering of ages suggests that a Lateglacial age for these landforms is reasonable and that the rockslide likely occurred very shortly after deglaciation. We therefore favor a 12–14 ka age for the glacial landforms at Dassu and Chakpo.

The difference in ages between the glacial landforms at Mungo and Biafo-Panmah, and at other locations for this glacial stage might reflect a lag time in the deglaciation and ice thinning between Mungo and Biafo-Panmah, and the other locations. Fig. 15 shows schematic glacier profiles and suggests progressive downwasting of a large valley glacier at ~13 and 11.4 ka. Alternatively, these data might represent two separate advances/readvance as the main valley glacier, with its confluencing glaciers, retreated from it 16 ka position. It is noteworthy that younger set of ages spans the Younger Dryas Stade. Taking the scattering of ages by >2 ka into account, the view that these moraines represent two distinct glacial advances is favored.

6.4. Askole glacial stage

The ^{10}Be TCN surface exposure ages for the Askole glacial stage moraines show that they date to ~5.7 and 0.8 ka. This indicates that the moraines likely formed during the middle Holocene and possibly the Little Ice Age. The ages on the latero-frontal moraine at Askole (m_{2G}) cluster around 5.7±0.5 ka (error = 1σ) with one outlier (K2-65–12.6±0.4 ka).

The hummocks near Skardu that we interpreted as moraines (m_{2B} in Figs. 3 and 4) have a TCN surface exposure age of 4.4±0.7 ka (error = 1σ). The deformed sediments beneath the diamict that comprises these hummocks that is exposed in the terraces at the K2 Motel have OSL ages of 7.4±0.6 (OSL K2-1) and 5.6±0.4 ka (OSL K2-2). The latter OSL age is from sediment higher in the section. These OSL ages support the TCN ages showing that the moraine formed after ~5 ka. The disturbance of the moraine surfaces by humans might account for a few hundred years difference between the youngest OSL age and the TCN ages.

The four sets of latero-frontal moraines near the present snout of the Biafo glacier have TCN surface exposure ages of 0.8±0.3 ka (error = 1σ) (Fig. 1H; m_{1H} in Fig. 12). Two samples (K2-34 and 35) could not be measured on the accelerator mass spectrometer due to too low concentration of ^{10}Be, which suggests that they are extremely young. Given the possibility of a few hundred years of inheritance, the boulders probably represent a LIA advance. However, the LIA is not well defined for the Himalaya. The data are important, however, because they support the view that inheritance of the glacial boulders is not significant (more than a few hundred years) in this region and TCN exposure ages in our studies are reasonable estimates of the true age of the moraines.

7. Discussion

This study broadly agrees with Owen's (1988) view that the possible planation and glacial benches in this region represent at least five major glacial advances. However, we group the glacier advances into four glacial stages. The ages of the younger three glacial stages have been defined

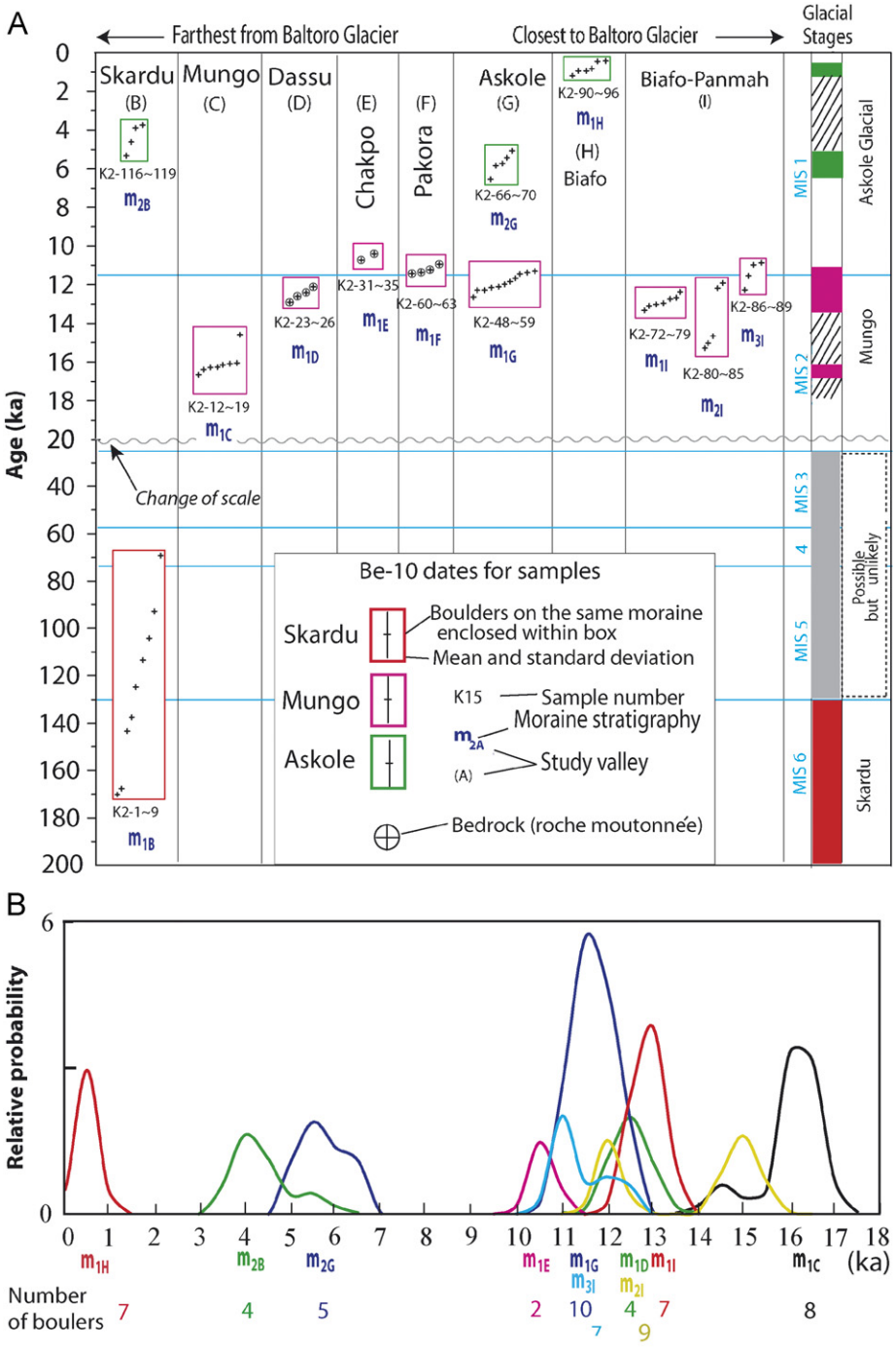

Fig. 14. ^{10}Be TCN surface exposure dates for boulders on the moraines dated from each of study areas: (A) scatter plots of ages on each moraine. Marine Oxygen Isotope Stages (MIS; after Martinson et al., 1987) are shown in light blue. Note that the vertical scale changes from 20 ka and its boundary is marked by light gray undulating line; (B) probability distributions for ^{10}Be TCN surface exposure dates of each glacial advance. Each different color represents an individual glacial landform.

by TCN surface exposure dating (Figs. 14 and 15; Table 1 and 2).

The oldest glacial stage (Bunthang) provides evidence suggesting that the Indus valley and its tributaries, which includes the Shigar valley, were filled with valley glaciers during the early Quaternary. These valleys were subsequently filled with glacier ice at least once more as testified by the moraines on top of Karpochi Rock, which belong to the Skardu glacial stage. These moraines may have formed during MIS 6, or more likely, during a much earlier glacial cycle. The top of mesa that includes Karpochi Rock, Bluko Rock, and Stronodoka Ridge probably mark the valley floor at that time.

Glaciers reached to at least the village of Mungo, >80 km from the present ice margins of the Baltoro glacier, during the Mungo glacial stage (Fig. 6). The glacier

at Mungo was ⩾1 km thick and would have comprised glaciers confluent with Baltoro glaciers, including the Biafo and Chogo Lungma glaciers. Given this thickness it is likely that glaciers extended down the Shigar valley to at least Shigar, where denuded lateral moraines are present to the immediate east of the village of Shigar. The diffluence col at the northern side of the Stronodoka ridge that contains moraines and till suggests that Shigar valley glacier may have reached the Skardu Basin during the Mungo glacial stage (Fig. 5). However, we did not date moraines within the diffluence col, and given that the height of the moraine on the col is comparable to the Karpochi Rock, it is possible that the col dates to the Skardu glacial stage. Subsequent to the deepening of the valleys, they were filled with a ~100 m-thick deposit of fluvial and lacustrine sediment, the remnants of which are well-preserved against what is now the mesa of Karpochi Rock during the Mungo glacial stage.

Valley glaciers from tributary valleys advanced into the Braldu valley during the Holocene (e.g. near Askole; Fig. 10C) to form moraines several tens of meters high. The hummocks in the Skardu Basin that have mid-Holocene TCN ages were interpreted by Hewitt (1999) to be the result of rock avalanching, whereas Owen (1988) and our field observations suggest that they are moraines that formed when a tributary glacier advanced over, and glaciotectonized the wet fluvial and lacustrine sediments that formed the lower terrace throughout the Skardu Basin (Owen, 1988; Fig. 4F). However, the low altitude of this moraine (~2270 m asl) and the lack of contemporary glaciers below at least 4500 m asl on the slopes to the south suggests that an equilibrium-line depression of ⩾1000 m would have been required to create these moraines during the Holocene. This is incompatible with current views on nature of climate change in the Holocene and contrasts with the equilibrium-line depression for the moraines at Askole, which is in the order of a few hundred meters. It is unlikely that both the TCN and OSL ages on the hummocks at Skardu are erroneous and therefore the young age would support Hewitt's (1999) view that these

Table 3
Summary of OSL dating results from quartz extracted from sediment sample: particle size, sample locations, radioisotope concentrations, cosmic dose rates, total dose-rates, D_E values and optical ages

Sample number	Particle size (μm)	Location (°N/°E)	Altitude (m asl.)	Depth (cm)	U[a] (ppm)	Th[a] (ppm)	K[a] (%)	Rb[a] (ppm)	Cosmic Dose rate[b] (mGya^{-1})	Total dose-rate[c,d] (mGya^{-1})	Number of aliquots[e]	Mean D_E[f] (Gy)	Age[g] (ka)
OSL K2-1	90–125	35.291°/ 75.661°	2274	160	2.35	14.0	1.83	110.0	0.24±0.02	3.24±0.19	24(26)	24.1±5.5	7.4±0.6
OSL K2-2	90–125	35.291°/ 75.661°	2274	140	2.19	14.1	2.16	125.0	0.25±0.03	3.50±0.21	23(26)	19.6±4.0	5.6±0.4

[a]Elemental concentrations from NAA of whole sediment measured at USGS Nuclear Reactor in Denver. Uncertainty taken as ±10%.
[b]Estimated contribution to dose-rate from cosmic rays calculated according to Prescott and Hutton (1994). Uncertainty taken as ±10%.
[c]Estimated fractional water content from whole sediment is 5±5%.
[d]Total dose-rate from beta, gamma and cosmic components. Beta attenuation factors for U, Th and K compositions incorporating grain size factors from Mejdahl (1979). Beta attenuation factor for Rb arbitrarily taken as 0.75 (cf. Adamiec and Aitken, 1998). Factors utilized to convert elemental concentrations to beta and gamma dose-rates from Adamiec and Aitken (1998) and beta and gamma components attenuated for moisture content.
[e]Number of aliquots measured. The number in parenthesis refers to the number of aliquots used to calculate the D_E.
[f]Mean equivalent dose (D_E) determined from replicated single-aliquot regenerative-dose (SAR; Murray and Wintle, 2000) runs. Errors are cited as 1 standard deviation.
[g]Errors are 1-sigma standard errors (i.e. $\sigma_{n-1}/n^{1/2}$) incorporating error from beta source estimated at about ±5%.

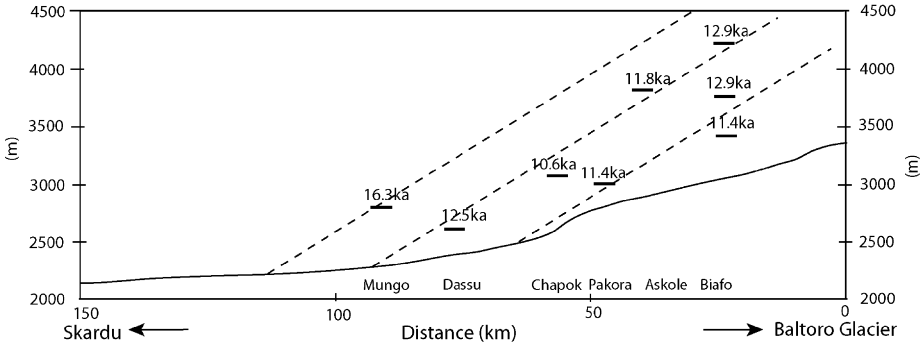

Fig. 15. Distribution of moraines formed during Mungo glacial stage. The dashed lines are schematic profiles of the main trunk glacier during the Mungo glacial stage. The profiles are based on the present gradient of the Baltoro Glacier. Three altitudinally distinct former ice limits are apparent. The highest ice limit dates to ~16 ka, while the lower two ice limits date to ~12–13 and ~11 ka, respectively. This suggests either progressive downwasting of the Baltoro trunk valley glacier or two readvances.

deposits are the result of rock avalanching. However, the complex deformation structures in the terraces still need further explanation to be attributed to the result of deformation due to rock avalanching. At this stage, therefore, we refrain from using this landform for glacial reconstructions until further geomorphic, sedimentological and geochronological studies have been undertaken on similar landforms in the Skardu Basin.

The present climate of the central Karakoram is dominated by mid-latitude westerlies with minor monsoonal influence. During low latitude insolation maxima, however, the climate was likely to be more influenced by variations in the intensity of the south Asian monsoon (Sirocko et al., 1991). This would lead to an increase and a farther-north penetration of monsoon-derived moisture, which in turn could result in positive glacier mass balances as precipitation falls as snow at high altitudes. In addition to changes in the Indian summer monsoon, cooling events associated with increased ice rafting events in the North Atlantic, Heinrich events during glacial times (Bond et al., 1992) and the Rapid Climate Changes of Bond et al. (1997, 2001) during the Lateglacial and the Holocene, could be teleconnected via the mid-latitude westerlies to the Transhimalaya resulting in glacial advances (Aizen et al., 2001; Barry and Chorley, 2003). In the Central Karakoram it is likely that glaciation is influenced by both oscillations in the south Asian monsoon and the mid-latitude westerlies. Making connection between glacial events and two climate systems and correlating the glacial successions in the Central Karakoram with specific dated climatic events is difficult because of the uncertainties related to the use of TCN surface exposure dating. Nevertheless, broad correlation can be made between regions and with climatic events.

The oldest glacial stage that was dated, the Skardu glacial, has TCN surface exposure ages that suggests that the moraines of this stage may have formed during MIS 6 or more likely in an earlier glacial cycle. The uncertainty of the age of this glacial stage makes it impossible to correlate with other regions of the Himalayan–Tibetan orogen. However, it is notable that glacial advances older than the last glacial cycle have been recognized in adjacent regions. These include the Karasu glacial stage of Muztag Ata–Kongur Shan (Seong et al., 2007a) and Leh glacial stage in Ladakh (Owen et al., 2006) that probably date to 127–305 and >400 ka, respectively. The lack of old dates throughout most Himalayan study areas may be the result of poor preservation, particularly in the more monsoon-influenced regions where fluvial and mass-movement processes are more dominant. Alternatively, it may be that in other regions, glaciation during the last glacial cycle was extensive enough to have destroyed evidence of early glaciations.

There is no glacial geologic evidence in the Central Karakoram for a glacier advance between MIS 5 through MIS 3. The lack of evidence for a glacial advance during the early part of the last glacial cycle is likely due to the poor preservation potential in this high energy environment as paraglacial and post-glacial processes easily rework and destroy glacial landforms. Barnard et al. (2003, 2004a, b, 2006), for example, showed how effective and efficient paraglacial processes are at reworking glacial and associated deposits in other regions of the Himalayan–Tibetan orogen. Alternatively the MIS 2 advances may have been more extensive and could have destroyed any evidence for glacial advances during MIS 5 through MIS 3. Given the records of glacial advance during the early part of the last glacial cycle in the adjacent areas, such as the Hunza Valley that has a similar climate regime, it is likely that glacial, paraglacial and post-glacial processes destroyed the evidence of former glacial deposits.

The Mungo glacial stage probably represents multiple glacial advances during the MIS 2. These glaciations resulted in the formation of well-preserved lateral moraines and roche moutonnées by thick valley glaciers along the Braldu valley. Glaciation during the Mungo glacial stage was less extensive than during the Skardu glacial stage. The tight cluster of ages allows us to tentatively assign the moraine at Mungo village (m_{1C} and m_{2C}) to Heinrich event 1. The younger ages of 11–13 ka on glacial landforms is possibly coincident with the Younger Dryas Stade. However, the span of Younger Dryas Stade is only 1300 years and given the uncertainty with production rates and weathering it is difficult to unequivocally assign these landforms to this climostratigrahic time. If the Mungo glacial stage advances occurred at these climostratigraphic times, this suggests that the glaciation in this region is likely to be associated with Northern Hemisphere cooling teleconnected by mid-latitude westerlies. Evidence for such teleconnections is provided by other climate proxies around the Tibetan Plateau, including the Chinese loess record (Porter and Zhou, 2006) and the Tibetan ice core records (Thompson et al., 1989). The combination of cooler temperatures with increased precipitation supplied by the mid-latitude westerlies, which brought moisture from the Mediterranean, Black Sea, Caspian Sea and Aral Sea, allowed the glaciers in the Central Karakoram to advance well into the main valley during the Mungo glacial stage. In addition to these teleconnections that affect the mid-latitude westerlies, evidence from numerical simulations suggests enhanced monsoon flow at 16 ka compared to the gLGM (Bush et al., 2007). Both summer and winter monsoons are stronger at 16 ka than at the gLGM with enhanced precipitation, particularly over the Karakoram. In this region it is likely that glaciation was influenced by changes in both the mid-latitude westerlies and the Indian summer monsoon.

The dated Askole glacial stage glacial landforms that are present within the region were examined in two different areas, Askole, and Biafo (m_{2G} and m_{1H} in Table 1). The glacial advances during the Askole glacial stage in the region might be synchronous with the Holocene Bond events 3 and 0, which are apparent in North Atlantic deep sea records (Bond et al., 2001). However, presently there is no other independent data for the Karakoram to support

significant climate change at these times and these correlations need to be more fully tested in future work. If these glacier advances are synchronous with Bond events then the lower temperature at these times, and the likely increased frequencies and magnitude of storm track development in the region might have increased the moisture supply to the region (Denton and Karlén, 1973; An and Porter, 1997; Alley and Ágústsdóttir, 2005; Porter and Zhou, 2006; Seong et al., 2007a), which in turn likely resulted in positive glacier mass balances, allowing glaciers to advance. This combination of relatively high winter accumulation and lower temperature may have helped drive the tributary glacial advance during the Holocene. Likewise, during the Little Ice Age, the total snow accumulation at Dasuopu ice sheet in southern Tibet was 30% higher than the summer amounts in northern India (Thompson, 2000). This was possibly the result of the increased winter snowfall as westerly low-pressure systems linked to the North Atlantic pushed farther east along the Himalaya than they normally do today. The increased albedo due to increased snowfall and the colder temperatures would have allowed excess snow to fall and persist late into each year. This in turn would have weakened the Indian summer monsoon.

Each successive glaciation in the study region became progressively less extensive, from >200 km long and >2 km thick valley glaciers to restricted (a few kilometers) tributary valley glacier advances. We cannot determine the reason for this pattern, but it might reflect a global pattern of progressively more restricted mountain glaciation throughout the Quaternary, or a more local control related to topographic constrains and/or uplift.

Correlating glacial advances between regions in the Himalayan–Tibetan orogen is difficult. Owen et al. (2005, 2006) suggested broad correlations between distant regions, but was limited by the accuracy and precision of the dating. We therefore refrain from detailed correlations with other areas of the Himalayan–Tibetan orogen. Our Central Karakoram study, however, highlights the striking contrasts in the extent of glaciation between neighboring regions. For example, in the Hunza valley, ~50 km NW of the K2-Baltoro region, glaciers did not advance more than a few kilometers during MIS 2 and 1 (Owen et al., 2002b), whereas in the K2-Baltoro region extensive valley glaciers advanced many tens of kilometers from their present positions during MIS 2. As our knowledge of the timing and extent of Quaternary glaciation in the Himalayan–Tibetan orogen improves, such as provided by our study, it may become possible to resolve the relative roles of difficult major climatic systems in forcing glaciation in Central Asia.

8. Conclusions

The geomorphology and ^{10}Be TCN chronology shows that glaciers in this region likely advanced during the early Quaternary (Bunthang glacial stage), MIS 6 or more likely during a much earlier glacial cycle (the Skardu glacial stage), MIS 2 (Mungo glacial stage), and the Holocene (Askole glacial stage). Our ^{10}Be TCN data for the Mungo glacial stage show that glaciers likely advanced at ~16 ka and between 13 and 11 ka. The former may represent a deglaciation age for the gLGM or it more likely represents a distinct advance broadly synchronous with ice-rafting events in the North Atlantic during the Heinrich event 1. The latter glacial advance (13–11 ka) might represent a deglaciation age for the former, but more likely represents a separate advance during the Younger Dryas Stade. The glacial advances during the Askole glacial stage might be in phase with the Holocene rapid climate changes, although the scattered ages and uncertainty with the TCN production rates and scaling factors cannot allow us to unequivocally assign them to climatic events. Our initial results suggest that the record of glacial advances in western Tibet supports the view that atmospheric teleconnections between the Tibet and the Northern Hemisphere ice sheets and oceans existed throughout the Late Quaternary. This is also consistent with earlier suggestions that changes in the physical oceanography of the North Atlantic Ocean affect the climate downwind, including the strength and path of storm tracks within the mid-latitude westerly system that passes over western Tibet, which in turn force glaciation. However, we cannot exclude a likely strong monsoonal influence. Our glacial chronology nevertheless provides a framework for future studies on paleo-environmental change and landscape evolution in Central Asia to help answer key questions regarding the nature of climate change and to test tectonic and geomorphic models for orogenic belts.

Acknowledgments

We would like to acknowledge the long-term and highly fruitful relationship with the late Syed Hamidullah, former Director of the Center of Excellence at Peshawar University, who did so much to help us with this project. We would also like to thank his students, Faisal Khan and Mohammad Shahid, for their excellent assistance in the field. Special thanks to the medics of University of Nebraska at Omaha, lead by Keith Brown and Bruce Hagen, for their support in the field. This research was supported by funding from the National Geographic Society and the US National Science Foundation (Grant BCS-0242339) to the University of Nebraska—Omaha and the University of Cincinnati. Part of this work was undertaken at the Lawrence Livermore National Laboratory (under DOE Contract W-7405-ENG-48). This research formed part of Y.B. Seong's doctoral research, which was partially supported by a Meyers Fellowship at the University of Cincinnati. Special thanks to Thomas Lowell for suggestions on an early draft of this paper, and Ed Brook, Alan Gillespie and an anonymous reviewer for their useful and constructive review.

References

Adamiec, G., Aitken, M., 1998. Dose-rate conversion factors: update. Ancient TL 16, 37–50.

Aizen, V., Aizen, E., 1997. Hydrological cycles on the north and south peripheries of mountain–glacial basins of Central Asia. Hydrological Processes 11, 451–469.

Aizen, E.M., Aizen, V.B., Melack, J.M., Nakamura, T., Ohta, T., 2001. Precipitation and atmospheric circulation patterns at mid-latitudes of Asia. International Journal of Climatology 21, 535–556.

Alley, R.B., Ágústsdóttir, A.M., 2005. The 8 ka event: cause and consequence of a major Holocene abrupt climate change. Quaternary Science Reviews 24, 1123–1149.

An, Z.S., Porter, S.C., 1997. Millennial-scale climatic oscillations during the last interglaciation in central China. Geology 25, 603–606.

Balco, G., Stone, J.O., 2007. A simple, internally consistent, and easily accessible means of calculating surface exposure ages or erosion rates from 10Be and 26Al measurements. Quaternary Geochronology, in press.

Barnard, P.L., Owen, L.A., Finkel, R.C., Asahi, K., 2003. Landscape response to deglaciation in a high relief, monsoon-influenced alpine environment, Langtang Himal, Nepal. Quaternary Science Reviews 25, 2162–2176.

Barnard, P.L., Owen, L.A., Finkel, R.C., 2004a. Style and timing of glacial and paraglacial sedimentation in a monsoonal influenced high Himalayan environment, the upper Bhagirathi Valley, Garhwal, Himalaya. Sedimentary Geology 165, 199–221.

Barnard, P.L., Owen, L.A., Sharma, M.C., Finkel., R.C., 2004b. Late Quaternary landscape evolution of a monsoon-influenced high Himalayan valley, Gori Ganga, Nanda Devi, NE Garhwal. Geomorphology 61, 91–110.

Barnard, P.L., Owen, L.A., Finkel, R.C., 2006. Quaternary fans and terraces in the Khumbu Himal south of Mount Everest: their characteristics, age and formation. Journal of Geological Society of London 163, 383–399.

Barry, R.G., Chorley, R.J., 2003. Atmosphere, Weather, and Climate, eighth ed. 279pp.

Benn, D.I., Owen, L.A., 2002. Himalayan glacial sedimentary environments: a framework for reconstructing and dating former glacial extents in high mountain regions. Quaternary International 97-98, 3–26.

Bond, G., Heinrich, H., Broecker, W., Labeyrie, L., Mc-Manus, J., Andrews, J., Huon, S., Jantschik, R., Clasen, S., Simet, C., Tedesco, K., Klas, M., Bonani, G., Ivy, S., 1992. Evidence for massive discharges of icebergs into the North Atlantic during the last glacial period. Nature 360, 245–249.

Bond, G., Showers, W., Cheseby, M., Lotti, R., Almasi, P., deMenocal, P., Priore, P., Cullen, H., Hajdas, I., Bonani, G., 1997. A pervasive millenial-scale cycle in North Atlantic Holocene and glacial climates. Science 278, 1257–1266.

Bond, G., Kromer, B., Beer, J., Muscheler, R., Evans, M., Showers, W., Hoffmann, S., Lotti-Bond, R., Hajdas, I., Bonani, G., 2001. Persistent solar influence on North Atlantic climate during the Holocene. Science 294, 2130–2136.

Burgisser, H.M., Gansser, A., Pika, J., 1982. Lateglacial lake sediments of the Indus Valley area, northwestern Himalayas. Eclogae Geologische Helvetica 75, 51–63.

Bush, A.B.G., Bishop, M., Copland, L., Kamp, U., Owen, L.A., Seong, Y.B., Shroder, J., Clendon, P., 2007. Himalayan climate at 16,000 years before present: changes in monsoon circulations and the westerlies, in preparation.

Cronin, V.S., 1989. Structural setting of the Skardu intermontane basin, Karakoram Himalaya, Pakistan. Geological Society of America Special Paper 232, 183–201.

Cronin, V.S., Johnson, W.P., Johnson, N.M., Johnson, G.D., 1989. Chronostratigraphy of the upper Cenozoic Bunthang sequence and possible mechanisms controlling base level in Skardu intermontane basin, Karakoram, Himalaya, Pakistan. Geological Society of America Special Paper 232, 295–309.

Denton, G.H., Karlén, W., 1973. Holocene climatic variations: their pattern and possible cause. Quaternary Research 3, 155–205.

Derbyshire, E., 1981. Glacier regime and glacial sediment facies: a hypothetical framework for the Qinghai-Xizang Plateau. In: Proceedings of Symposium on Qinghai-Xizang (Tibet) Plateau, vol. 2. Beijing, China. Science Press, Beijing, Geological and Ecological studies of Qinghai-Xizang Plateau. pp. 1649–1656.

Derbyshire, E., Owen, L.A., 1990. Quaternary alluvial fans in the Karakoram Mountains. In: Rachocki, A.H., Church, M. (Eds.), Alluvial Fans: A Field Approach. Wiley, Chichester, pp. 27–53.

Dianelli, G., 1922. Studi sul glaciale Spedizone Italian de Filippi nell' Himalaia, Caracorume Turchestan/Cinese (1913–1914). Ser. II, 3, p.658.

Drew, F., 1873. Alluvial and lacustrine deposits and glacial records of the upper Indus basin. Part 1: alluvial deposits. Geological Society of London Quarterly Journal 29, 449–471.

Finkel, R.C., Owen, L.A., Barnard, P.L., Caffee, M.W., 2003. Beryllium-10 dating of Mount Everest moraines indicates a strong monsoonal influence and glacial synchroniety throughout the Himalya. Geology 31, 561–564.

Foster, D.A., Gleadow, A.J.W., Mortimer, G., 1994. Rapid Pliocene exhumation in the Karakoram (Pakistan), revealed by fission-track thermochronology of the K2 gneiss. Geology 22, 19–22.

Hewitt, K., 1989. The altitudinal organisation of Karakoram geomorphic processes and depositional environments. Zeitschrift für Geomorphologie, N.F. Suppl.-Bd 76, 9–32.

Hewitt, K., 1998. Catastrophic landslides and their effects on the Upper Indus streams, Karakoram Himalaya, northern Pakistan. Geomorphology 26, 47–80.

Hewitt, K., 1999. Quaternary moraines vs. catastrophic avalanches in the Karakoram Himalaya, northern Pakistan. Quaternary Research 51, 220–237.

Hewit, K., 2005. The Karakoram anomaly? Glacier Expansion and the 'Elevation Effect,' Karakoram Himalaya. Mountain Research and Development 25, 332–340.

Kohl, C.P., Nishiizumi, K., 1992. Chemical isolation of quartz for measurement of in situ produced cosmogenic nuclides. Geochimica et Cosmochimica Acta 56, 3583–3587.

Lal, D., 1991. Cosmic ray labeling of erosion surfaces: in situ nuclide production rates and erosion models. Earth and Planetary Science Letters 104, 429–439.

Lal, D., Harris, N.B.W., Sharma, K.K., Gu, Z., Ding, L., Liu, T., Dong, W., Caffee, M.W., Jull, A.J.T., 2003. Erosion history of the Tibetan Plateau since the Last Interglacial: constrains from the first studies of cosmogenic ^{10}Be from Tibetan bedrock: Earth and Planetary Science Letters 217, 33–42.

Meihe, G., Winiger, M., Böhner, J., Yili, Z., 2001. Climatic diagram map of High Asia 1: purpose and concepts. Erdkunde 55, 94–97.

Mejdahl, V., 1979. Thermoluminescence dating: beta attenuation in quartz grains. Archaeometry 21, 61–73.

Murray, A.S., Wintle, A.G., 2000. Luminescence dating of quartz using an improved single-aliquot regenerative-dose protocol. Radiation Measurements 32, 57–73.

Nishiizumi, K., Winterer, E.L., Kohl, C.P., Lal, D., Arnold, J.R., Klein, J., Middleton, R., 1989. Cosmic ray production rates of ^{10}Be and ^{26}Al in quartz from glacially polished rocks. Journal of Geophysical Research 94 (B12), 17,907–17,915.

Olley, J.M., Caitcheon, G.G., Roberts, R.G., 1999. The origin of dose distributions in fluvial sediments, and the prospect of dating single grains from fluvial deposits using optically stimulated luminescence. Radiation Measurements 30, 207–217.

Owen, L.A., 1988. Wet-sediment deformation of Quaternary and recent sediments in the Skardu Basin, Karakoram Mountains, Pakistan. In: Croot (Ed.), Glaciotectonics: Forms and Processes. Balkema, Rotterdam, pp. 123–148.

Owen, L.A., Derbyshire, E., 1988. Glacially deformed diamictons in the Karakoram Mountains, northern Pakistan. In: Croot (Ed.), Glaciotectonics: Forms and Processes. Balkema, Rotterdam, pp. 149–176.

Owen, L.A., Derbyshire, E., 1989. The Karakoram glacial depositional system. Zeitschrift für Geomorphologie 76, 33–73.

Owen, L.A., Gualtieri, L., Finkel, R.C., Caffee, M.W., Benn, D.I., Sharma, M.C., 2001. Cosmogenic radionuclide dating of glacial landforms in the Lahul Himalaya, northern India: defining the timing of Late Quaternary glaciation. Journal of Quaternary Science 16, 555–563.

Owen, L.A., Finkel, R.C., Caffee, M.W., 2002a. A note on the extent of glaciation in the Himalaya during the global Last Glacial Maximum. Quaternary Science Reviews 21, 147–157.

Owen, L.A., Finkel, R.C., Caffee, M.W., Gualtieri, L., 2002b. Timing of multiple Late Quaternary glaciations in the Hunza Valley, Karakoram Mountains, northern Pakistan: defined by cosmogenic radionuclide dating of moraines. Geological Society of America Bulletin 114, 593–604.

Owen, L.A., Kamp, U., Spencer, J.Q., Haserodt, K., 2002c. Timing and style of Late Quaternary glaciation in the eastern Hindu Kush, Chitral, northern Pakistan: a review and revision of the glacial chronology based on new optically stimulated luminescence dating. Quaternary International 97–98, 41–55.

Owen, L.A., Spencer, J.Q., Ma, H., Barnard, P.L., Derbyshire, E., Finkel, R.C., Caffee, M.W., Zeng, Y.N., 2003a. Timing of Late Quaternary glaciation along the southwestern slopes of the Qilian Shan, Tibet. Boreas 32, 281–291.

Owen, L.A., Finkel, R.C., Ma, H., Spencer, J.Q., Derbyshire, E., Barnard, P.L., Caffee, M.W., 2003b. Timing and style of Late Quaternary glaciations in NE Tibet. Geological Society of America Bulletin 115, 1356–1364.

Owen, L.A., Finkel., R.C., Barnard, P.L., Haizhhou, M., Asahi, K., Caffee, M.W., Derbyshire, E., 2005. Climatic and topographic controls on the style and timing of Late Quaternary glaciation throughout Tibet and the Himalaya defined by 10Be cosmogenic radionuclide surface exposure dating. Quaternary Science Reviews 24, 1391–1411.

Owen, L.A., Caffee, M.W., Bovard, K.R., Finkel, R.C., Sharma, M.C., 2006. Terrestrial cosmogenic nuclide surface exposure dating of the oldest glacial successions in the Himalayan orogen. Ladakh Range, northern India. Geological Society of America Bulletin 118, 383–392.

Owen, L.A., Bright, J., Finkel, R.C., Jaiswal, M.K., Kaufman, D.S., Mahan, S., Radtke, U., Schneider, J.S., Sharp, W., Singhvi, A.K., Warren, C.N., 2007. Numerical dating of a Late Quaternary spit-shoreline complex at the northern end of Silver Lake playa, Mojave Desert, California: a comparison of the applicability of radiocarbon, luminescence, terrestrial cosmogenic nuclide, electron spin resonance, U-series and amino acid racemization methods. Quaternary International 166, 87–110.

Paffen, K.H., Pillewizer, W., Schneide, H.J., 1956. Forschungen im Hunza-Karakoram. Erdkunde 10, 1–33.

Phillips, W.M., Sloan, V.F., Shroder Jr., J.F., Sharma, P., Clarke, M.L., Rendell, H.M., 2000. Asynchronous glaciation at Nanga Parbat, northwestern Himalaya Mountains, Pakistan. Geology 28, 431–434.

Porter, S.C., Zhou, W., 2006. Synchronism of Holocene East Asian monsoon variations and North Atlantic drift-ice tracers. Quaternary Research 65, 443–449.

Prescott, J.R., Hutton, J.T., 1994. Cosmic ray contributions to dose rates for luminescence and ESR dating: Large depths and long-term time variations. Radiation Measurements 23, 497–500.

Richards, B.W.M., Owen, L.A., Rhodes, E.J., 2000a. Timing of Late Quaternary glaciations in the Himalayas of northern Pakistan. Journal of Quaternary Science 15, 283–297.

Richards, B.W.M., Benn, D., Owen, L.A., Rhodes, E.J., Spencer, J.Q., 2000b. Timing of Late Quaternary glaciations south of Mount Everest in the Khumbu Himal, Nepal. Geological Society of America Bulletin 112, 1621–1632.

Searle, M.P., 1991. Geology and Tectonics of the Karakoram Mountains. Wiley, Chichester, 358pp.

Seong, Y.B., Owen, L.A., Yi, Y., Finkel, C.R., 2007a. Quaternary glaciation of Muztag Ata and Kongur Shan: evidence for glacier response to rapid climate changes throughout the Lateglacial and Holocene in westernmost Tibet. Geological Society of America Bulletin, in review.

Seong, Y.B., Owen, L.A., Bishop, M.P., Bush, A., Clendon, P., Copland, L., Finkel, R.C., Kamp, U., Shroder, J.F., 2007b. Rates of fluvial bedrock incision within an actively uplifting orogen: Central Karakoram Mountains, northern Pakistan. Geomorphology, in press.

Sharma, M.C., Owen, L.A., 1996. Quaternary glacial history of the Garhwal Himalaya, India. Quaternary Science Reviews 15, 335–365.

Shi, Y., 2002. Characteristics of late Quaternary monsoonal glaciation on the Tibetan Plateau and in East Asia. Quaternary International 97–98, 79–91.

Shroder, J., Bishop, M., Bush, A., Copeland, L., Kamp, U., Owen, L.A., Seong, Y.B., Weeks, P., 2007. Postglacial slope failure and denudation in the Central Karakoram (tentative), in preparation.

Sirocko, F., Sarnthein, M., Lango, H., Erlenkeuser, H., 1991. The atmospheric summer circulation and coastal upwelling in the Arabian Sea during the Holocene and the last glaciation. Quaternary Research 36, 72–73.

Small, E.E., Anderson, R.S., Repka, J.L., Finkel, R.C., 1997. Erosion rates of alpine bedrock summit surfaces deduced from in situ Be-10 and Al-26. Earth and Planetary Science Letters 150, 413–425.

Spencer, J.Q., Owen, L.A., 2004. Optically stimulated luminescence dating of Late Quaternary glaciogenic sediments in the upper Hunza valley: validating the timing of glaciation and assessing dating methods. Quaternary Sciences Reviews 23, 175–191.

Stone, J.O., 2000. Air pressure and cosmogenic isotope production. Journal of Geophysical Research 105, 23753–23759.

Thompson, L.G., 2000. Ice core evidence for climate change in the Tropics: implications for our future. Quaternary Science Reviews 19, 19–35.

Thompson, L.G., Mosley-Thompson, E., Davis, M.E., Bolzan, J.F., Dai, J., Yao, T., Gundestrup, N., Wu, X., Klein, L., Xie, Z., 1989. Holocene–Late Pleistocene climatic ice core records from Qinghai-Tibetan Plateau. Science 246, 474–477.

Tsukamoto, S., Asahi, K., Watanabe, T., Kondo, R., Rink, W.J., 2002. Timing of past glaciation in Kanchenjunga Himal, Nepal by optically stimulated luminescence dating of tills. Quaternary International 97/98, 57–68.

Wake, C.P., 1987. Snow accumulation studies in the central Karakoram. In: Proceedings of the Eastern Snow Conference, vol. 44, 1987, pp. 19–33.

Wake, C.P., 1989. Glaciochemical investigations as a tool for determining the spatial and seasonal variation of snow accumulation in the central Karakoram, northern Pakistan. Annals of Glaciology 13, 279–284.

Wallinga, J., 2002. Optically stimulated luminescence dating of fluvial deposits: a review. Boreas 31, 303–322.

Zehfuss, P.H., Bierman, P.R., Gillespie, A.R., Burke, R.A., Caffee, M.C., 2001. Slip rates on the Fish Springs fault, Owens Valley, California, deduced from cosmogenic 10Be and 26Al and soil development on fan surfaces. Geological Society of America Bulletin 113, 241–255.